



Simonetti, B., Cullen, P. J., Xavier, R., & et al. (2020). Sorting nexin 5 mediates virus-induced autophagy and immunity. *Nature*, 589, 456–461. <https://doi.org/10.1038/s41586-020-03056-z>

Peer reviewed version

Link to published version (if available):
[10.1038/s41586-020-03056-z](https://doi.org/10.1038/s41586-020-03056-z)

[Link to publication record in Explore Bristol Research](#)
PDF-document

This is the author accepted manuscript (AAM). The final published version (version of record) is available online via Springer Nature at <https://doi.org/10.1038/s41586-020-03056-z>. Please refer to any applicable terms of use of the publisher.

University of Bristol - Explore Bristol Research

General rights

This document is made available in accordance with publisher policies. Please cite only the published version using the reference above. Full terms of use are available: <http://www.bristol.ac.uk/red/research-policy/pure/user-guides/ebr-terms/>

1
2 **Sorting Nexin 5 Mediates Virus-Induced Autophagy and Immunity**
3

4 Xiaonan Dong¹, Yuting Yang¹, Zhongju Zou^{1,2}, Yuting Zhao¹, Bo Ci³, Lin Zhong³, Madhura
5 Bhawe⁴, Liwei Wang⁵, Yi-Chun Kuo⁵, Xiao Zang³, Rui Zhong³, Elizabeth R. Aguilera⁶, R. Blake
6 Richardson⁶, Boris Simonetti⁷, John W. Schoggins⁶, Julie K. Pfeiffer⁶, Li Yu⁸, Xuewu Zhang⁵,
7 Yang Xie^{3,9}, Sandra L. Schmid⁴, Guanghua Xiao^{3,9}, Paul A. Gleeson¹⁰, Nicholas T. Ktistakis¹¹,
8 Peter J. Cullen⁷, Ramnik J. Xavier^{12,13,14,*} and Beth Levine^{1,2,6}

9 ¹Center for Autophagy Research, Department of Internal Medicine, University of Texas
10 Southwestern Medical Center, Dallas, Texas 75390, USA

11 ²Howard Hughes Medical Institute, University of Texas Southwestern Medical Center, Dallas,
12 Texas 75390, USA

13 ³Quantitative Biomedical Research Center, Department of Population and Data Sciences,
14 University of Texas Southwestern Medical Center, Dallas, Texas 75390, USA

15 ⁴Department of Cell Biology, University of Texas Southwestern Medical Center, Dallas, Texas
16 75390, USA

17 ⁵Department of Pharmacology, University of Texas Southwestern Medical Center, Dallas, Texas
18 75390, USA

19 ⁶Department of Microbiology, University of Texas Southwestern Medical Center, Dallas, Texas
20 75390, USA

21 ⁷School of Biochemistry, University of Bristol, Bristol BS8 1TD, UK

22 ⁸The State Key Laboratory of Membrane Biology, Tsinghua University-Peking University Joint
23 Centre for Life Sciences, School of Life Sciences, Tsinghua University, Beijing 100084, China

24 ⁹Harold C. Simmons Comprehensive Cancer Center, University of Texas Southwestern Medical
25 Center, Dallas, Texas 75390, USA

26 ¹⁰Department of Biochemistry and Molecular Biology and Bio21 Molecular Science and
27 Biotechnology Institute, The University of Melbourne, Victoria 3010, Australia

28 ¹¹Signalling Programme, The Babraham Institute, Cambridge CB22 4AT, UK

29 ¹²Center for Computational and Integrative Biology, Massachusetts General Hospital, Harvard
30 School of Medicine, Boston, Massachusetts 02114, USA

31 ¹³Department of Molecular Biology, Massachusetts General Hospital and Harvard Medical
32 School, Boston, Massachusetts 02114, USA

33 ¹⁴Broad Institute of MIT and Harvard University, Cambridge, Massachusetts 02142, USA

34 *Correspondence to: xavier@molbio.mgh.harvard.edu

35 **Autophagy, a lysosomal degradation pathway, plays an essential role in multiple aspects of**
36 **immunity, including immune system development, regulation of innate and adaptive**
37 **immune and inflammatory responses, selective degradation of intracellular microbes, and**
38 **host protection against infectious diseases^{1,2}. Unlike autophagy induction by stimuli such as**
39 **nutrient deprivation and mTOR suppression, little is known about how autophagosomal**
40 **biogenesis is initiated in mammalian cells in response to viral infection. We performed**
41 **genome-wide siRNA screens and found that the endosomal protein sorting nexin 5**
42 **(SNX5)^{3,4} is essential for virus-induced, but not for basal, stress- or endosome-induced,**
43 **autophagy. We showed that *SNX5* deletion increases cellular susceptibility to viral infection**
44 ***in vitro*, and that *Snx5* knockout in mice enhances lethality after infection with multiple**
45 **human viruses. Mechanistically, SNX5 interacts with beclin 1 and ATG14-containing Class**
46 **III phosphatidylinositol 3-kinase (PI3KC3) complex 1 (PI3KC3-C1), increases the lipid**
47 **kinase activity of purified PI3KC3-C1, and is required for endosomal generation of PI3P**
48 **and recruitment of the PI3P-binding protein WIPI2 to virion-containing endosomes. These**
49 **findings identify a context- and organelle-specific mechanism – SNX5-dependent PI3KC3-**
50 **C1 activation at endosomes – for autophagy initiation during viral infection.**

51 To identify cellular factors required for virus-induced autophagy, we performed high-content
52 image-based genome-wide siRNA screens in HeLa cells infected with Sindbis virus (SIN) (an
53 enveloped single-stranded RNA virus) and a genetically engineered strain of herpes simplex
54 virus type 1 (HSV-1) (an enveloped double-stranded DNA virus). The latter contains a deletion
55 in the beclin 1-binding domain (BBD) of the HSV-1 neurovirulence protein ICP34.5 that
56 prevents it from inhibiting host autophagy (HSV-1 Δ BBD)⁵. The autophagy pathway targets these
57 viruses *in vitro*, protecting mice against lethal central nervous system (CNS) infection⁵⁻⁷. Both

58 viruses induce autophagy in HeLa and HeLa/GFP-LC3 cells as demonstrated by increased GFP-
59 LC3 (a marker of autophagosomes) puncta, increased conversion of LC3-I to the lipidated
60 autophagosome-associated form LC3-II; and degradation of the autophagy substrate
61 p62/SQSTM1 (Extended Data Fig. 1a-i). These changes reflect autophagic flux, as GFP-LC3
62 puncta and LC3-II accumulation increased further upon lysosomal inhibition with bafilomycin
63 A1, which also decreased p62/SQSTM1 degradation. This autophagic flux was reduced by
64 siRNA knockdown of essential autophagy genes *ATG7* and *ATG13*, as well as pharmacological
65 inhibition with the Class III phosphatidylinositol-3 kinase (PI3KC3, also known as PIK3C3 or
66 VPS34) inhibitor, PIK-III (Extended Data Fig. 1). These results indicate a role for the autophagy
67 protein conjugation systems, the autophagy-initiating ULK1 complex and the PI3KC3 complex,
68 involved in autophagosome membrane nucleation, in virus-induced autophagy.

69 Primary screens of a pooled siRNA oligonucleotide library targeting 18,115 unique human
70 genes showed that knockdown of 310 genes resulted in fewer GFP-LC3 puncta in SIN- and/or
71 HSV-1 Δ BBD-infected HeLa/GFP-LC3 cells but not in mock-infected cells (Extended Data Fig.
72 2a-e). We performed deconvolution screens with four individual siRNA oligonucleotides per
73 candidate gene. Gene knockdown with two or more siRNA oligonucleotides decreased numbers
74 of virus-induced GFP-LC3 puncta for 216 of 310 (69.7%) genes (confirmed hits) (Fig. 1a,
75 Extended Data Fig. 2f, g).

76 Bioinformatic analyses showed enrichment for gene sets associated with biological processes
77 and molecular functions, including protein complex assembly, transport, kinases and certain
78 transcription factors (Extended Data Fig. 2h, i), as well as NLRX1 which promotes virus-induced
79 autophagy⁸. We focused on endosomal proteins, as most viruses enter cells through a route that
80 converges at the endolysosomal system⁹. Cytoplasmic entry of SIN and HSV-1 Δ BBD via fusion

81 at the plasma membrane resulted in fewer GFP-LC3 puncta than normal entry (Extended Data
82 Fig. 3a-d), underscoring the importance of endosomal entry for virus-induced autophagy. We
83 focused further analyses on the endosomal protein sorting nexin 5 (SNX5). SNX5 encodes a
84 predicted Phox (PX) domain, a conserved protein domain that binds phosphoinositides, such as
85 phosphatidylinositol 3-phosphate (PI3P). Additionally, SNX5 contains a Bin/Amphiphysin/Rvs
86 (BAR) domain, which is essential for sensing and driving membrane curvature^{10,11}. Critical early
87 events during autophagosomal biogenesis include PI3P generation by the PI3KC3 complex I
88 (PI3KC3-C1, also known as PIK3C3-C1) and membrane remodeling¹². Thus, we hypothesized
89 that SNX5 might act during viral endosomal entry to increase endosome-based PI3P generation
90 and initiate autophagosome formation.

91 Knockdown of *SNX5*, and the related gene *SNX32*, decreased SIN- and HSV-1ΔBBD-
92 induced autophagy by a magnitude similar to *ATG7* knockdown (Fig. 1b, Extended Data Fig. 3e-
93 i). Importantly, siRNA knockdown of *SNX5* or *SNX32* decreased autophagy induction by six
94 additional pathogenic human viruses, including Zika virus¹³, West Nile virus (WNV)¹⁴,
95 chikungunya virus (CHIKV)¹⁵, poliovirus¹⁶, Coxsackievirus B3 (CVB3)¹⁷ and influenza A virus
96 (IAV)¹⁸ (Fig. 1b, Extended Data Fig. 3e-i). To rule out off-target siRNA effects, we generated
97 HeLa *SNX5*^{KO} cells using the CRISPR/Cas9 system and stably transfected them with GFP-LC3
98 (Extended Data Fig. 3j). *SNX5*^{KO}/GFP-LC3 cells were deficient in SIN- and HSV-1ΔBBD-
99 induced autophagy, but this defect was fully rescued by reconstitution of wild-type SNX5 in two
100 independent *SNX5*^{KO}/GFP-LC3/*SNX5* cell clones (Extended Data Fig. 3k). These results indicate
101 that SNX5 is required for autophagy induced by a broad range of viral pathogens.

102 Neither siRNA knockdown of *SNX5* or *SNX32*, nor CRISPR knockout of *SNX5*, altered basal
103 autophagy, starvation-induced autophagy, or mTOR inhibition-induced autophagy (Extended

104 Data Fig. 4a-c). *SNX5*^{KO} and wild-type HeLa/GFP-LC3 cells showed identical formation of LC3-
105 positive Group A *Streptococcus* containing vacuoles¹⁹ (Extended Data Fig. 4d, e), indicating that
106 xenophagy of a bacterium that enters cells by endosomes does not require SNX5. SNX5 was also
107 dispensable for osmotic stress-induced LC3-recruitment to endolysosomal structures labeled by
108 EEA1 and LAMP1²⁰ (Extended Data Fig. 4f, g). Furthermore, *SNX5*^{KO} and wild-type HeLa cells
109 exhibited similar monensin-induced LC3 recruitment to latex bead-containing phagosomes, an
110 assay for measuring LC3-associated phagocytosis (LAP) in non-phagocytic cells²¹ (Extended
111 Data Fig. 4h, i). Thus, SNX5 is specific for virus-induced autophagy, and is not required for
112 general autophagy or non-canonical forms of autophagy that require endolysosomal or
113 phagosomal LC3 recruitment.

114 siRNA knockdown of the essential retromer gene *VPS29* did not alter virus-induced
115 autophagy (Fig. 1b, Extended Data Fig. 3e, h), but impaired retromer-dependent retrograde
116 transport of glucose transporter 1 (GLUT1) as demonstrated by increased lysosomal localization
117 of mis-sorted GLUT1 (Extended Data Fig. 5a-f). Consistent with the reported functional
118 redundancy of SNX5, SNX6 and SNX32 in retromer activity^{4,22}, neither knockdown of *SNX5* nor
119 *SNX32* impaired GLUT1 trafficking. Early endocytic function was identical in *SNX5*^{KO} and wild-
120 type HeLa cells, as measured by recycling kinetics of the transferrin receptor (Extended Data
121 Fig. 5g-i). Late endocytic function also remained unchanged in *SNX5*^{KO} cells, as measured by
122 rates of epidermal growth factor receptor (EGFR) degradation (Extended Data Fig. 5j, k). Thus,
123 the requirement for SNX5 in virus-induced autophagy is unlikely related to a role in retromer
124 function or other endocytic functions.

125 Since autophagy restricts the replication of certain viruses *in vitro* and protects against
126 certain viral diseases *in vivo*^{1,2}, we studied viral infection in SNX5-deficient cells and

127 pathogenesis in *Snx5*^{-/-} mice²³. We focused on SIN, HSV-1ΔBBD, WNV, and CHIKV viruses for
128 which existing data indicate the importance of autophagy in controlling viral disease^{5-7,15,24,25}.
129 For the first three, which are neuronotropic and cause fatal encephalitis in mice, we used an
130 intracranial model of *in vivo* infection to study virus-host interactions in neurons without
131 confounding effects of other stages of pathogenesis, including viral dissemination from the
132 periphery and systemic immune responses that do not penetrate the blood-brain barrier. For
133 CHIKV, we used an established model of peripheral viral infection in neonatal mice, as previous
134 studies have reported a protective role of autophagy^{15,25}. *SNX5* deletion in HeLa cells increased
135 susceptibility to SIN, HSV-1ΔBBD, WNV and CHIKV infection in viral infectivity assay
136 (Extended Data Fig. 6a-d). Viral multi-step growth also increased in *SNX5*^{KO} cells (Extended
137 Data Fig. 6e-h), as well as in primary mouse embryonic fibroblasts (MEFs) derived from *Snx5*^{-/-}
138 compared to wild-type littermates (Extended Data Fig. 6i-l). Viral infectivity and replication was
139 not increased in *SNX5*^{KO} cells or *Snx5*^{-/-} MEFs after infection with autophagy-suppressing
140 viruses, including SIN.dnAtg5 (expressing a dominant negative Atg5) and HSV-1ΔBBD-MR (a
141 marker-rescued strain of HSV-1ΔBBD expressing wild-type ICP34.5, which inhibits host
142 autophagy by binding beclin 1) (Extended Data Fig. 6m-r). Increased viral replication in *SNX5*
143 deficiency was not due to alterations in viral entry (Extended Data Fig. 6s, t) or virus-induced
144 interferon signaling (Extended Data Fig. 6u, v), and *SNX5* mRNA did not decrease upon
145 infection (Extended Data Fig. 6w). Therefore, *SNX5* restricts viral replication in a cell
146 autonomous fashion by an autophagy-dependent mechanism.

147 Neonatal *Snx5*^{-/-} mice were more susceptible to lethal infection with SIN, CHIKV, or WNV
148 than *Snx5*^{+/+} counterparts, and adult *Snx5*^{-/-} mice were more susceptible to lethal HSV-1ΔBBD
149 encephalitis than their wild-type littermates (Fig. 1c). The brains of neonatal SIN-infected and

150 adult HSV-1 Δ BBD-infected *Snx5*^{-/-} mice revealed increased viral titers and neuronal death at
151 certain time points after infection (Extended Data Fig. 7a-f). This *Snx5*-mediated protective
152 effect is likely related to autophagy induction, as mortality did not differ between *Snx5*^{+/+} and
153 *Snx5*^{-/-} mice infected with SIN.dnAtg5 or HSV-1 Δ BBD-MR that inhibit neuronal autophagy^{5,6}
154 (Fig. 1c, Extended Data Fig. 7g). Thus, *Snx5* is a previously undescribed host factor that
155 functions in antiviral defense *in vivo*.

156 We evaluated whether SNX5 interacts with autophagy-specific PI3KC3-C1 complexes,
157 which function in autophagosome initiation or PI3KC3-C2 complexes, which function in
158 autophagosome maturation and endocytic trafficking¹². As demonstrated by the presence of
159 ATG14, but not UVRAG (Fig. 2a), only PI3KC3-C1 complexes co-immunoprecipitated with
160 SNX5. This difference is not due to alterations in assembled PI3KC3-C1 or PI3KC3-C2
161 complexes, as both ATG14 and UVRAG co-immunoprecipitated with beclin 1 (Fig. 2b). The
162 SNX5-PI3KC3-C1 interaction does not require PI3KC3-C1 lipid kinase activity, as it is not
163 diminished by treatment with the PI3KC3-specific inhibitor PIK-III (Fig. 2a, b), which blocks
164 autophagy during baseline conditions, starvation, mTOR inhibition, and viral infection
165 (Extended Data Figs. 11, 8a-e). Recombinant SNX5 interacts with intact PI3KC3-C1, but not
166 PI3KC3-C2, complexes (Fig. 2c-e, Extended Data Fig. 8f), indicating a direct SNX5-PI3KC3-C1
167 interaction. The interaction specificity may represent binding of SNX5 to the PI3KC3-C1-
168 specific protein ATG14, an autophagy protein that senses membrane curvature²⁶, or other
169 conformational differences between PI3KC3-C1 and PI3KC3-C2^{27,28}.

170 Our findings suggest that SNX5 acts upstream of PI3P generation to regulate PI3KC3-C1
171 activation during viral infection. We therefore studied the effects of recombinant SNX5 on the
172 lipid kinase activity of Large Unilamellar Vesicles prepared by Extrusion Technique

173 (LUVETs)^{29,30} with two distinct membrane curvatures employing a lipid mixture that resembles
174 endosomal lipid composition^{31,32}. On smaller LUVETs, PI3KC3-C1 complexes exhibited
175 approximately three-fold higher lipid kinase activity which was abolished by PIK-III (Fig. 2f).
176 Compared to SUMO control protein (Fig. 2c), recombinant SUMO-SNX5 increased PI3KC3-C1
177 activity on larger LUVETs in a dose-dependent manner (Fig. 2g, left); the magnitude of this
178 effect was decreased on smaller LUVETs with greater membrane curvature (Fig. 2g, right).

179 Positively charged residues in the concave surface of BAR domains mediate membrane
180 association of BAR-containing proteins via electrostatic interaction with the lipid bilayer¹¹.
181 K429E, K430E and R431E mutations in the BAR domain of SNX1, a sorting nexin closely
182 related to SNX5, block its association with membranes and the ability to induce membrane
183 remodeling³³. To investigate whether the corresponding positively charged BAR domain
184 residues in SNX5 are required for its effect on PI3KC3-C1 activity, we aligned amino acid
185 sequences of SNX5 and SNX1 and identified residues K328, R330 and K332, which were
186 substituted with glutamic acid (SNX5 EEE) (Extended Data Fig. 8g, h). Unlike wild-type
187 SUMO-SNX5, the EEE mutant protein failed to enhance PI3KC3-C1 activity on larger LUVETs
188 (Fig. 2g). SUMO-SNX5 EEE did not bind PI3KC3-C1 complexes (Fig. 2e), indicating that the
189 tip region of the BAR domain carrying these evolutionarily conserved residues is required for
190 interaction with PI3KC3-C1. A previous study revealed that PI3KC3-C1 has diminished capacity
191 to generate PI3P on low-curvature membranes such as giant unilamellar vesicles²⁸. Our data
192 suggest that SNX5, by enhancing local membrane curvature through its BAR domain, facilitates
193 PI3KC3-C1-mediated PI3P generation on flatter membranes that resemble the endosome.

194 We next performed cryogenic electron microscopy (cryo-EM) of the larger LUVETs
195 incubated with SUMO-SNX5, SUMO-SNX5 EEE or SUMO control protein. In the presence of

196 SNX5, but not SUMO-SNX5 EEE, liposomes had increased membrane curvature (Fig. 2h, i).
197 Thus, at least *in vitro*, the SNX5 BAR domain is required for increasing liposomal membrane
198 curvature, a mechanism essential for increased PI3KC3-C1 activity.

199 Virally-infected *SNX5*^{KO} cells were defective in endosomal PI3P production, as measured
200 both by staining with a fluorescent PI3P-binding probe, PX-Alexa555²⁸, and immunostaining for
201 WIPI2, a PI3P-binding protein and early autophagosome marker³⁴. Defects occurred during SIN
202 and HSV-1 Δ BBD infection, but not at baseline, or upon induction of autophagy by starvation or
203 mTOR inhibition. The PI3P production defect was rescued by wild-type SNX5 but not mutant
204 SNX5 EEE (Extended Data Fig. 9). SIN and HSV-1 Δ BBD infection increased WIPI2 puncta that
205 colocalized with EEA1 in parental wild-type and *SNX5*^{KO} cells reconstituted with wild-type
206 SNX5, but not in *SNX5*^{KO} cells or *SNX5*^{KO} cells reconstituted with SNX5 EEE (Fig. 3a, b). The
207 defect in endosomal WIPI2 puncta formation in *SNX5*^{KO} cells was not related to decreased
208 endosomal localization of beclin 1, ATG14 or VPS34 (Extended Data Fig. 10a). Similar to GFP-
209 LC3 puncta (Extended Data Fig. 11), the SIN- and HSV-1 Δ BBD-induced increase of the PI3P
210 probe signal and WIPI2 puncta formation in HeLa cells was abolished by PIK-III (Extended
211 Data Fig. 10b-e). Thus, SNX5 – and residues in its BAR domain predicted to sense and drive
212 membrane curvature – are not required for the endosomal localization of PI3KC3-C1, but are
213 required for the endosomal function of PI3KC3-C1 and PI3P generation in virally-infected cells.

214 To determine the location of SNX5-dependent PI3KC3-C1 activation, we employed a
215 Sindbis virus strain expressing mCherry fused to the E2 envelope glycoprotein (SIN.mCherry-
216 E2)³⁵. One hour after infection, SIN.mCherry-E2 was present in EEA1-positive endosomes,
217 representing endocytosed virions (Fig. 3c). An increased percentage of mCherry-E2-positive
218 EEA1-positive structures with colocalized SNX5 puncta relative to mCherry-E2-negative EEA1-

219 positive structures (Fig. 3c-e) indicates selective recruitment of SNX5 to virion-containing
220 endosomes. Similarly, more colocalized WIPI2 puncta (Fig. 3f, g) indicates the selective
221 generation of PI3P at virion-containing endosomes. WIPI2 puncta formation at virion-containing
222 endosomes decreased in SIN.mCherry-E2-infected *SNX5*^{KO} cells; this defect was rescued by
223 wild-type SNX5 but not SNX5 EEE (Fig. 3f, g). Thus, SNX5 functions specifically at virion-
224 containing endosomes to increase PI3KC3-C1 activity and autophagosomal biogenesis.

225 Our findings suggest that stimuli inside an organelle may be linked to organelle-specific
226 initiation of autophagosomal biogenesis. When viruses enter endosomes, SNX5, a protein that
227 senses and drives membrane curvature, specifically localizes to virion-containing early
228 endosomes and functions to initiate activation of the ATG14-containing PI3KC3-C1 complex,
229 the first stage of autophagosome formation. This mechanism is unique to viral infections and not
230 to other forms of stress-induced autophagy (e.g. nutrient deprivation and mTOR inhibition) or
231 non-canonical forms of autophagy (e.g. bacterial xenophagy, osmotic stress-induced autophagy
232 and LAP), suggesting distinct cellular mechanisms for activating PI3KC3-C1 and autophagy in
233 response to different stress stimuli. We speculate that as-of-yet unidentified proteins that regulate
234 membrane curvature (or other factors that locally govern PI3KC3-C1 activity) serve as crucial
235 mediators of stimulus-specific autophagy.

236 The question of how luminal viruses stimulate the SNX5-PI3KC3 axis on the cytoplasmic
237 face of endosomes remains outstanding. Based on insights from other experimental systems²²,
238 SNX5 may associate with an array of integral membrane proteins to establish a “signature” for
239 virion-containing endosomes. Evidence that the human cytomegalovirus tegument protein UL35
240 antagonizes SNX5-mediated antiviral activity³⁶ and that SIN replication is attenuated in *SNX5*^{KO}
241 HEK293T cells³⁷ suggests evolutionarily conserved complex mechanisms by which SNX5

242 mediates host-virus interactions. Additional structural and microscopy-based studies, requiring
243 development of specific immuno-electron microscopy-based tools, will be needed to capture the
244 transient interaction of SNX5 with virion-containing endosomal membranes and to dissect the
245 precise molecular mechanisms underlying this process.

246

247 **References:**

- 248 1. Levine, B., Mizushima, N. & Virgin, H. W. Autophagy in immunity and inflammation.
249 *Nature* **469**, 323-335 (2011).
- 250 2. Dong, X. & Levine, B. Autophagy and viruses: adversaries or allies? *J Innate Immun* **5**,
251 480-493 (2013).
- 252 3. Merino-Trigo, A. *et al.* Sorting nexin 5 is localized to a subdomain of the early
253 endosomes and is recruited to the plasma membrane following EGF stimulation. *J Cell*
254 *Sci* **117**, 6413-6424 (2004).
- 255 4. Wassmer, T. *et al.* A loss-of-function screen reveals SNX5 and SNX6 as potential
256 components of the mammalian retromer. *J Cell Sci* **120**, 45-54 (2007).
- 257 5. Orvedahl, A. *et al.* HSV-1 ICP34.5 confers neurovirulence by targeting the Beclin 1
258 autophagy protein. *Cell Host Microbe* **1**, 23-35 (2007).
- 259 6. Orvedahl, A. *et al.* Autophagy protects against Sindbis virus infection of the central
260 nervous system. *Cell Host Microbe* **7**, 115-127 (2010).
- 261 7. Sumpter, R., Jr. *et al.* Fanconi anemia proteins function in mitophagy and immunity. *Cell*
262 **165**, 867-881 (2016).
- 263 8. Lei, Y. *et al.* The mitochondrial proteins NLRX1 and TUFM form a complex that
264 regulates type I interferon and autophagy. *Immunity* **36**, 933-946 (2012).

- 265 9. Mercer, J., Schelhaas, M. & Helenius, A. Virus entry by endocytosis. *Annu Rev Biochem*
266 **79**, 803-833 (2010).
- 267 10. Mim, C. & Unger, V. M. Membrane curvature and its generation by BAR proteins.
268 *Trends Biochem Sci* **37**, 526-533 (2012).
- 269 11. Gallop, J. L. & McMahon, H. T. BAR domains and membrane curvature: bringing your
270 curves to the BAR. *Biochem Soc Symp* **72**, 223-231 (2005).
- 271 12. Levine, B., Liu, R., Dong, X. & Zhong, Q. Beclin orthologs: integrative hubs of cell
272 signaling, membrane trafficking, and physiology. *Trends Cell Biol* **25**, 533-544 (2015).
- 273 13. Liu, Y. *et al.* Inflammation-induced, STING-dependent autophagy restricts Zika virus
274 infection in the Drosophila brain. *Cell Host Microbe* **24**, 57-68 (2018).
- 275 14. Kobayashi, S. *et al.* Autophagy inhibits viral genome replication and gene expression
276 stages in West Nile virus infection. *Virus Res* **191**, 83-91 (2014).
- 277 15. Joubert, P. E. *et al.* Chikungunya virus-induced autophagy delays caspase-dependent cell
278 death. *J Exp Med* **209**, 1029-1047 (2012).
- 279 16. Jackson, W. T. *et al.* Subversion of cellular autophagosomal machinery by RNA viruses.
280 *PLoS Biol* **3**, e156 (2005).
- 281 17. Alirezaei, M., Flynn, C. T., Wood, M. R. & Whitton, J. L. Pancreatic acinar cell-specific
282 autophagy disruption reduces coxsackievirus replication and pathogenesis in vivo. *Cell*
283 *Host Microbe* **11**, 298-305 (2012).
- 284 18. Gannage, M. *et al.* Matrix protein 2 of influenza A virus blocks autophagosome fusion
285 with lysosomes. *Cell Host Microbe* **6**, 367-380 (2009).
- 286 19. Nakagawa, I. *et al.* Autophagy defends cells against invading group A Streptococcus.
287 *Science* **306**, 1037-1040 (2004).

- 288 20. Florey, O., Gammoh, N., Kim, S. E., Jiang, X. & Overholtzer, M. V-ATPase and osmotic
289 imbalances activate endolysosomal LC3 lipidation. *Autophagy* **11**, 88-99 (2015).
- 290 21. Fletcher, K. *et al.* The WD40 domain of ATG16L1 is required for its non-canonical role
291 in lipidation of LC3 at single membranes. *EMBO J* **37**, e97840 (2018).
- 292 22. Simonetti, B., Danson, C. M., Heesom, K. J. & Cullen, P. J. Sequence-dependent cargo
293 recognition by SNX-BARs mediates retromer-independent transport of CI-MPR. *J Cell*
294 *Biol* **216**, 3695-3712 (2017).
- 295 23. Lim, J. P., Gosavi, P., Mintern, J. D., Ross, E. M. & Gleeson, P. A. Sorting nexin 5
296 selectively regulates dorsal-ruffle-mediated macropinocytosis in primary macrophages. *J*
297 *Cell Sci* **128**, 4407-4419 (2015).
- 298 24. Yordy, B., Iijima, N., Huttner, A., Leib, D. & Iwasaki, A. A neuron-specific role for
299 autophagy in antiviral defense against herpes simplex virus. *Cell Host Microbe* **12**, 334-
300 345 (2012).
- 301 25. Shoji-Kawata, S. *et al.* Identification of a candidate therapeutic autophagy-inducing
302 peptide. *Nature* **494**, 201-206 (2013).
- 303 26. Fan, W., Nassiri, A. & Zhong, Q. Autophagosome targeting and membrane curvature
304 sensing by Barkor/Atg14(L). *Proc Natl Acad Sci U S A* **108**, 7769-7774 (2011).
- 305 27. Baskaran, S. *et al.* Architecture and dynamics of the autophagic phosphatidylinositol 3-
306 kinase complex. *Elife* **3**, e05115 (2014).
- 307 28. Rostislavleva, K. *et al.* Structure and flexibility of the endosomal Vps34 complex reveals
308 the basis of its function on membranes. *Science* **350**, aac7365 (2015).
- 309 29. Hope, M. J., Bally, M. B., Webb, G. & Cullis, P. R. Production of large unilamellar
310 vesicles by a rapid extrusion procedure: characterization of size distribution, trapped

311 volume and ability to maintain a membrane potential. *Biochim Biophys Acta* **812**, 55-65
312 (1985).

313 30. Mayer, L. D., Hope, M. J. & Cullis, P. R. Vesicles of variable sizes produced by a rapid
314 extrusion procedure. *Biochim Biophys Acta* **858**, 161-168 (1986).

315 31. Evans, W. H. & Hardison, W. G. Phospholipid, cholesterol, polypeptide and glycoprotein
316 composition of hepatic endosome subfractions. *Biochem J* **232**, 33-36 (1985).

317 32. Kobayashi, T. *et al.* A lipid associated with the antiphospholipid syndrome regulates
318 endosome structure and function. *Nature* **392**, 193-197 (1998).

319 33. Carlton, J. *et al.* Sorting nexin-1 mediates tubular endosome-to-TGN transport through
320 coincidence sensing of high- curvature membranes and 3-phosphoinositides. *Curr Biol*
321 **14**, 1791-1800 (2004).

322 34. Polson, H. E. *et al.* Mammalian Atg18 (WIPI2) localizes to omegasome-anchored
323 phagophores and positively regulates LC3 lipidation. *Autophagy* **6**, 506-522 (2010).

324 35. Jose, J., Tang, J., Taylor, A. B., Baker, T. S. & Kuhn, R. J. Fluorescent protein-tagged
325 Sindbis virus E2 glycoprotein allows single particle analysis of virus budding from live
326 cells. *Viruses* **7**, 6182-6199 (2015).

327 36. Maschkowitz, G., Gartner, S., Hofmann-Winkler, H., Fickenscher, H. & Winkler, M.
328 Interaction of human cytomegalovirus tegument proteins ppUL35 and ppUL35A with
329 sorting nexin 5 regulates glycoprotein B (gpUL55) localization. *J Virol* **92**, e00013-18
330 (2018).

331 37. Schuchman, R. *et al.* Comparative Characterization of the Sindbis virus proteome from
332 mammalian and invertebrate hosts identifies nsP2 as a component of the virion and

333 sorting nexin 5 as a significant host factor for alphavirus replication. *J Virol* **92**, e00694-
334 18 (2018).

335

336 **Acknowledgments:** This work was supported by Cancer Prevention Research Institute of Texas
337 (CPRIT) grants RP120718 (B.L.) and RP180805 (Y.X.), NIH U19 AI109725 (B.L., R.X.), NIH
338 U19 AI142784 (B.L., R.X.), NIH R01 DK097485 (R.X.), NIH R35 GM130289 (X.Z.), NIH R01
339 GM115473 (Y.X.), NIH R01 CA172211 (G.X.), the Welch Foundation grant I-1702 (X.Z.), the
340 Rita Allen Foundation (J.W.S.) the Biotechnology and Biological Sciences Research Council
341 grant BB/K019155/1 (N.T.K.), and National Health and Medical Research Council Australia
342 (NHMRC) APP1163862 (P.A.G.). We thank Herbert W. Virgin, Rhea M. Sumpter Jr., Anthony
343 Orvedahl, Milton Packer, David A. Leib, Jennifer Lippincott-Schwartz, Sharon Tooze, Sarah
344 Cherry, Kate Luby-Phelps, Lisa N. Kinch, Chad A. Brautigam, Diana Tomchick, Michael Roth,
345 Michael Shiloh and John Neff for helpful discussions; Melissa Johnson, Hanspeter
346 Niederstrasser and Bruce Posner for assistance with siGENOME siRNA library; Luequn Huang
347 for assistance with high-throughput siRNA screens and data analysis; Yohei Ohashi and Michael
348 Wilson for the design of the PX domain probe and Maria Manifava for assistance in PI3P
349 staining; Abhijit Bugde and the UT Southwestern Medical Center (UTSW) Live Cell Imaging
350 Facility for assistance with fluorescence microscopy; Zhe Chen and Yang Li from the Structural
351 Biology Laboratory at UTSW for assistance with cryo-EM studies (supported in part by CPRIT
352 grant RP170644); Michael S. Diamond, Michael Gale Jr., Adolfo Garcia-Sastre, Deborah J.
353 Lenschow, Karla Kirkegaard, Marco Vignuzzi, Sharon Tooze, Diane E. Griffin, Richard J. Kuhn,
354 Ichiro Nakagawa, Ilya Bezprozvanny, Matthew B. Frieman, Charles M. Rice and Hongwei

355 Wang for providing critical reagents; Lori Nguyen for assistance with animal experiments; and
356 Haley Smith and Heather Kang for assistance with manuscript preparation.

357
358 **Author contributions:** X.D. and B.L. designed the study; X.D., Y.K., B.S., J.W.S., J.K.P., L.Y.,
359 X.Z., S.L.S., P.A.G., N.T.K., P.J.C., R.J.X. and B.L. developed methodology; Y.Z. purified
360 PI3KC3-C1 and PI3KC3-C2 complexes; L.W. purified SNX5 proteins; M.B. performed
361 transferrin receptor recycling assay and EGFR endolysosomal degradation assay; E.R.A. and
362 R.B.R. performed infection with CVB3, poliovirus, IAV and Zika virus; X.D., Y.Y. and Z.Z.,
363 performed animal study, viral growth curves, GFP-LC3 puncta quantitation, co-IP experiments
364 and western blot experiments; X.D. performed siRNA screens and all the other experiments in
365 this study; X.D., B.C., L.Z., X.Z., R.Z., Y.X., and G.X. analyzed the data; X.D. and B.L. wrote
366 the manuscript; R.J.X. contributed to and supervised the manuscript resubmission. Beth Levine
367 passed away in June 2020.

368
369 **Competing interests:** Beth Levine is a scientific co-founder of Casma Therapeutics, Inc.
370 Ramnik J. Xavier is co-founder of Jnana Therapeutics and Celsius Therapeutics. None of these
371 companies provided support for this work.

372

373 **Figure Legends**

374 **Fig. 1. SNX5 is required for virus-induced autophagy *in vitro* and antiviral host defense *in***
375 ***vivo*.** **a**, Confirmed hits from deconvolution siRNA screens grouped according to their
376 requirement for SIN-induced autophagy, HSV-1 Δ BBD-induced autophagy, or both. **b**, GFP-LC3
377 puncta in HeLa/GFP-LC3 cells treated with indicated siRNAs (72 h) and mock-infected or
378 infected with indicated virus for 4.5 h. MOI = 5 for HSV-1 Δ BBD; 10 for SIN, Zika virus, WNV,
379 CHIKV and IAV; and 20 for poliovirus and CVB3. Bars represent mean \pm s.d. of three
380 independent replicates (100-150 cells per sample). *P*-values, one-way ANOVA with Dunnett's
381 test for multiple comparisons. **c**, Survival of *Snx5*^{+/+} and *Snx5*^{-/-} mice infected with SIN (strain
382 dsTE12Q, 1,000 pfu i.c., 7-day-old mice), SIN.dnAtg5 (1,000 pfu i.c., 7-day-old mice), HSV-
383 1 Δ BBD (50,000 pfu i.c., 8 to 10-week-old mice), HSV-1 Δ BBD-MR (50,000 pfu i.c., 8 to 10-
384 week-old mice), WNV (1 pfu i.c., 5.5-day-old mice) or CHIKV (100,000 pfu s.c., 7-day-old
385 mice). Results represent combined data for at least three independent experiments per virus;
386 similar results obtained for each infection. *P*-values, log-rank test (two-sided).

387

388 **Fig. 2. SNX5 interacts with PI3KC3-C1 complex and augments its lipid kinase activity.** **a, b**,
389 Western blots showing co-immunoprecipitation of endogenous PI3KC3 complex proteins with
390 SNX5 (**a**) or beclin 1 (**b**) in HeLa cells treated with DMSO or PIK-III (5 μ M, 1 h). IP,
391 immunoprecipitates; WCL, whole cell lysates. **c, d**, Coomassie blue staining of His-tagged
392 SUMO, SUMO-SNX5 or SUMO-SNX5 EEE (**c**) or PI3KC3 complexes purified from HEK293F
393 cells co-transfected with plasmids expressing beclin 1, VPS34, VPS15 and either ATG14
394 (PI3KC3-C1) or UVRAG (PI3KC3-C2) (**d**). **e**, Western blot of His-tagged proteins in eluates
395 from *in vitro* binding with PI3KC3 complexes. Similar results for **a-e** were observed in three

396 independent experiments. **f**, Relative PI3KC3-C1 activity in an *in vitro* lipid kinase assay using
397 either PI⁻ or PI⁺ LUVETs +/- PIK-III (0.5 mM). Bars represent mean ± s.d., n=4 biologically
398 independent samples. *P*-values, unpaired two-tailed *t*-tests. PI3KC3-C1 has higher activity on
399 smaller PI⁺ LUVETs (*P* = 2.1e-8; two-way ANOVA). **g**, Relative PI3KC3-C1 activity
400 (normalized to 0 nM SUMO) in an *in vitro* lipid kinase assay using PI⁺ LUVETs with indicated
401 SUMO-fusion protein. Symbols represent mean ± s.d., n=4 biologically independent samples.
402 The dose-dependent SUMO-SNX5-mediated increase in lipid kinase activity is greater on larger
403 LUVETs (*P* = 0.000035; linear regression with three-way interaction term). **h**, **i**, Representative
404 cryo-EM micrographs (**h**) and violin plots of the radius of curvature for vertex points (**i**) of larger
405 PI⁺ LUVETs incubated for 30 min with buffer alone or indicated proteins (>150 liposomes per
406 sample). Scale bar, 60 nm. *P*-values, one-way ANOVA with Dunnett's test for multiple
407 comparisons. See Supplementary Fig. 1 for gel source data.

408

409 **Fig. 3. SNX5 is required for virus-induced endosomal generation of PI3P.** **a**, **b**,
410 Representative fluorescent micrographs (**a**) and quantitation (**b**) of WIPI2⁺ (green) and EEA1⁺
411 (red) puncta in indicated cells. Scale bars, 20 μm. Arrows denote representative WIPI2⁺EEA1⁺
412 puncta (white) that would score positive in **b**. Insets, 4X magnification of boxed areas. Error
413 bars, mean ± s.d. (three replicates, 100-150 cells each). **c-e**, Representative fluorescent
414 micrographs (**c**) and quantitation (**d**, **e**) of SNX5 endosomal localization in SIN.mCherry-E2-
415 infected HeLa cells (MOI = 10, 1 h). Scale bars, 20 μm. Boxed areas are magnified 9X (right) to
416 show SNX5 (green), E2 (red) and EEA1 (magenta) and SNX5⁺E2⁺EEA1⁺ colocalization
417 (yellow). Arrows and arrowheads denote representative SNX5⁺E2⁻EEA1⁺ and SNX5⁺E2⁺EEA1⁺
418 endosomes, respectively. Bars in **d** represent mean ± s.d. of Manders' overlap coefficient of

419 SNX5 and E2⁺EEA1⁺ or E2⁻EEA1⁺ colocalization (n=10, >40 cells per replicate). **e**, Violin plots
420 of percentage of overlapping SNX5⁺ and E2⁺EEA1⁺ or E2⁻EEA1⁺ puncta (n=137 cells). **f**, **g**,
421 Representative fluorescent micrographs (**f**) and quantitation (**g**) of endosomal WIPI2 puncta in
422 indicated cells. Scale bars, 20 μm. Boxed areas are magnified 4X (right) to show WIPI2 (green),
423 E2 (red) and EEA1 (magenta) and WIPI2⁺E2⁺EEA1⁺ colocalization (yellow). Yellow puncta
424 represent WIPI2⁺E2⁺EEA1⁺ puncta that would score positive in **g**. Bars in **g** represent mean ±
425 s.d. (n=3, 100-150 cells per replicate). *P*-values, one-way ANOVA with Dunnett's test for
426 multiple comparisons (**b**, **g**) or unpaired two-tailed *t*-test (**d**, **e**). Similar results obtained from
427 three independent experiments.

428

429 **Extended Data Figure Legends**

430 **Extended Data Fig. 1. SIN and HSV-1 Δ BBD increase autophagy in HeLa cells via an**
431 **ATG7-, ATG13-, and PI3KC3-dependent mechanism. a-c,** Representative fluorescent
432 micrographs (**a**) and quantitation (**b, c**) of GFP-LC3 puncta (autophagosomes) in HeLa/GFP-
433 LC3 cells treated with non-targeting control siRNA (NC) or *ATG7* siRNA for 72 h and then
434 mock-infected or infected with SIN or HSV-1 Δ BBD (at a multiplicity of infection [MOI] of 10
435 and 5, respectively; 4.5 h) in the presence or absence of the lysosomal inhibitor bafilomycin A1
436 (Baf A1, 100 nM) for 1 h prior to fixation. Scale bars, 20 μ m. Arrows denote representative
437 autophagosomes that would be scored as positive in **b** and **c**. The box plot with whiskers from
438 minimum to maximum in **b** represents 100-150 cells analyzed for one of triplicate samples per
439 condition. Bars in **c** represent mean \pm s.d. of triplicate samples (100-150 cells analyzed per
440 sample). Similar results were observed in three independent experiments. Both analyses were
441 performed for similar fluorescence microscopy experiments in Figs. 1, 3, and Extended Data
442 Figs. 1, 3, 4, 8, 9, 10, and only bar graphs are shown. **d,** Western blot analyses of indicated
443 proteins in HeLa/GFP-LC3 cells treated with NC or *ATG7* siRNA for 72 h as in **a-c**. **e-g,**
444 Representative western blot detection (**e**) and quantitation (**f, g**) of indicated proteins in lysates
445 (prepared with Triton X-100 lysis buffer) of HeLa cells mock-infected or infected with SIN or
446 HSV-1 Δ BBD (MOI = 10 and 5, respectively; 7 h) with the presence or absence of Baf A1 (100
447 nM) for 2 h (from 5 hours post infection [hpi] to 7 hpi). Bars in **f** and **g** represent mean \pm s.d. of
448 LC3-II/LC3-I ratios (**f**) and p62/actin ratios (**g**) of three independent experiments, respectively.
449 **h, i,** Representative western blot detection (**h**) and quantitation (**i**) of p62 and actin in lysates
450 (prepared with SDS lysis buffer) of HeLa cells mock-infected or infected with SIN or HSV-
451 1 Δ BBD (MOI = 10 and 5, respectively; 7 h). Bars in **i** represent mean \pm s.d. of p62/actin ratios of

452 three independent experiments. **j**, Quantitation of GFP-LC3 puncta in HeLa/GFP-LC3 cells
453 treated with NC or *ATG13* siRNA for 72 h and then mock-infected or infected with SIN or HSV-
454 1ΔBBD (MOI = 10 and 5, respectively; 4.5 h). **k**, Western blot analyses of indicated proteins in
455 HeLa/GFP-LC3 cells treated with NC or *ATG13* siRNA for 72 h as in **j**. **l**, Quantitation of GFP-
456 LC3 puncta in HeLa/GFP-LC3 cells mock-infected or infected with SIN or HSV-1ΔBBD (MOI
457 = 10 and 5, respectively; 4.5 h) and treated with PIK-III (5 μM), Baf A1 (100 nM) or DMSO
458 control for 1 h (from 3.5 hpi to 4.5 hpi). Bars in **j** and **l** represent mean ± s.d. of triplicate samples
459 (100-150 cells analyzed per sample). Similar results were observed in three independent
460 experiments. Unpaired two-tailed *t*-tests were used to compare means of Baf A1- versus DMSO-
461 treated cells, those of *ATG13* siRNA- versus NC-treated cells, and those of PIK-III- versus
462 DMSO-treated cells. One-way ANOVA with Dunnett's test for multiple comparisons was used
463 to compare means of SIN or HSV-1ΔBBD infection versus mock infection. For gel source data,
464 see Supplementary Fig. 1.

465

466 **Extended Data Fig. 2. Schematic summary, statistical analyses and functional enrichment**
467 **analyses of genome-wide siRNA screens. a**, Flowchart summary of primary and deconvolution
468 siRNA screens in HeLa/GFP-LC3 cells. Three filters were applied in the primary siRNA screens:
469 (1) absence of cytotoxicity of siRNA pools in transfected cells; (2) lack of effect of siRNA pools
470 on numbers of GFP-LC3 puncta in mock-infected cells (basal autophagy); and (3) significant
471 reduction of numbers of GFP-LC3 puncta in cells infected with either SIN or HSV-1ΔBBD
472 (virus-induced autophagy). In the deconvolution siRNA screens, positive hits were defined as
473 those genes with two or more individual siRNA oligonucleotides from siRNA pools that
474 reproduced the phenotype of the siRNA pools. **b-d**, Ranked distribution of median scores for

475 each siRNA pool in primary siRNA screens. Dots shown in graphs denote median scores of
476 GFP-LC3 puncta in mock-infected cells (**b**), SIN-infected cells (**c**) and HSV-1 Δ BBD-infected
477 cells (**d**). **e**, A representative receiver operating characteristic (ROC) curve of quality control
478 plates for primary and deconvolution screens. The ROC mean \pm s.d. of all the quality control
479 plates was 0.97 ± 0.03 , which indicates accuracy and specificity in the identification of cellular
480 factors that regulate numbers of GFP-LC3 puncta. **f**, Scatter plot of median scores of 216
481 confirmed hits from the deconvolution siRNA screens (open circles) and 40 negative on-plate
482 controls (open triangles). Scores are medians from triplicate assay plates of four individual
483 siRNA oligonucleotides per gene. The 216 confirmed hits and 40 negative on-plate controls fall
484 into two distinct clusters. **g**, Gene list from deconvolution screens for virus-induced autophagy
485 during infection with Sindbis virus (S) and HSV-1 Δ BBD (H). Numbers denote number of
486 individual siRNA oligonucleotides that scored positive in each screen. Green, genes with 2 or
487 more positive siRNA oligonucleotides (confirmed hits); magenta, genes with <2 positive siRNA
488 oligonucleotides (non-confirmed hits). **h**, Enrichment analyses of gene sets including molecular
489 function, biological process, cellular component and protein domain categories (terms) from
490 DAVID Bioinformatics Resources. There were 174 terms (open triangles) that contain at least
491 two confirmed hits and have hypergeometric test *P*-values less than 0.05; fourteen of these terms
492 exhibited false discovery rate (FDR) adjusted *P*-values less than 0.05. The enrichment score was
493 defined as $-\log_{10}$ (hypergeometric test *P*-value). **i**, Fourteen highly enriched terms plotted as a
494 network graph. Each node represents a gene set from a variety of categories (indicated in
495 brackets) as follows: G, GOTERM; I, INTERPRO; P, PIR_SUPERFAMILY, U,
496 UP_SEQ_FEATURE. The size of each node corresponds to the number of confirmed siRNA hits
497 and the color intensity is scaled according to the enrichment score. The thickness and color

498 intensity of lines connecting two nodes correspond to the extent of overlapping genes between
499 two gene sets. See Fig. 1a and Supplementary Tables 1 to 5 for further details.

500

501 **Extended Data Fig. 3. Impaired autophagy induction by acid-mediated bypass of endocytic**
502 **viral entry, confirmation of indicated gene knockdown in HeLa cells, and requirement for**
503 **SNX5 in autophagy induced by diverse viruses. a, b,** Representative fluorescent micrographs
504 **(a)** and quantitation **(b)** of GFP-LC3 puncta in HeLa/GFP-LC3 cells that were either mock-
505 infected or infected with SIN or HSV-1 Δ BBD (MOI = 50 and 25, respectively; 4.5 h) in the
506 presence (pH 5.4) or absence (pH 7.4) of an acidic pulse (that induces viral entry at the plasma
507 membrane) after viral attachment. Arrows in **a** denote representative GFP-LC3 puncta that
508 would be scored as positive in **b**. Scale bars, 20 μ m. Bars in **b** represent mean \pm s.d. of triplicate
509 samples (100-150 cells analyzed per sample). **c, d,** Viral entry efficiency in HeLa/GFP-LC3 cells
510 treated similarly as in **a** and **b**. Bars in **c** and **d** represent mean \pm s.d. of SIN minus-strand RNA
511 levels **(c)** and HSV-1 immediate early gene *ICP27* mRNA levels **(d)** of triplicate samples at
512 indicated time points, respectively. **e,** Representative fluorescent micrographs of GFP-LC3
513 puncta in HeLa/GFP-LC3 cells that were treated with indicated siRNAs (72 h) and then either
514 mock-infected or infected with indicated virus for 4.5 h (MOI = 10 for SIN, Zika virus, WNV,
515 CHIKV and IAV; MOI = 5 for HSV-1 Δ BBD; and MOI = 20 for poliovirus and CVB3). Scale
516 bars, 20 μ m. Arrows in **e** denote representative GFP-LC3 puncta that would be scored as positive
517 in Fig. 1b. **f-i,** Confirmation of gene knockdown in indicated siRNA-treated HeLa/GFP-LC3
518 cells (72 h) by western blot analyses of indicated proteins **(f-h)** or quantitative real-time PCR of
519 *SNX32* **(i)** for the experiment shown in Fig. 1b. Bars in **i** represent mean \pm s.d. of triplicate
520 samples. **j,** Western blot detection of SNX5 and actin in wild-type HeLa/GFP-LC3 cells (WT),

521 HeLa *SNX5*^{KO}/GFP-LC3 cells (KO), and two clones of reconstituted HeLa *SNX5*^{KO}/GFP-
522 LC3/*SNX5* cells used in the experiment shown in **k**. In **b**, one-way ANOVA with Dunnett's test
523 for multiple comparisons was used to compare means of SIN or HSV-1ΔBBD infection versus
524 mock infection. In **b-d**, unpaired two-tailed *t*-tests were used to compare means of pH7.4 versus
525 pH5.4 conditions. For **e-h, j**, similar results were observed in three independent experiments. In
526 **i**, an unpaired two-tailed *t*-test was used to compare means of NC versus *SNX32* knockdown. **k**,
527 GFP-LC3 puncta in reconstituted HeLa *SNX5*^{KO}/GFP-LC3 cells mock-infected or infected with
528 SIN or HSV-1ΔBBD (MOI = 10 and 5, respectively; 4.5 h). Bars represent mean ± s.d. of three
529 independent replicates (100-150 cells per sample). *P*-values, one-way ANOVA with Dunnett's
530 test for multiple comparisons. For gel source data, see Supplementary Fig. 1.

531

532 **Extended Data Fig. 4. *SNX5* is dispensable for general autophagy or non-canonical forms**
533 **of autophagy that require LC3 recruitment to endolysosomal or phagosomal compartments**
534 **in HeLa cells. a, b**, Representative fluorescent micrographs (**a**) and quantitation (**b**) of GFP-LC3
535 puncta in HeLa/GFP-LC3 cells that were treated with indicated siRNA (72 h) and then cultured
536 in normal medium (1 h), starvation medium (EBSS; 1 h), or normal medium containing torin 1
537 (250 nM; 1 h). Scale bars, 20 μm. Arrows denote representative autophagosomes that would be
538 scored as positive in **b**. **c**, Quantitation of GFP-LC3 puncta in wild-type HeLa/GFP-LC3 cells
539 (WT), HeLa *SNX5*^{KO}/GFP-LC3 cells (KO), and two clones of reconstituted HeLa *SNX5*^{KO}/GFP-
540 LC3/*SNX5* cells that were cultured in normal medium (1 h), starvation medium (EBSS; 1 h), or
541 normal medium containing torin 1 (250 nM; 1 h). **d, e**, Representative fluorescent micrographs
542 (**d**) and quantitation (**e**) of wild-type HeLa/GFP-LC3 cells and HeLa *SNX5*^{KO}/GFP-LC3 cells
543 bearing Group A *Streptococcus*-containing autophagosome-like vacuoles (GcAVs) at 2 h post

544 bacterial infection (MOI = 100) with Group A *Streptococcus* strain JRS4 and the isogenic mutant
545 JRS4 Δ SLO (which does not induce formation of GcAVs due to defective bacterial escape from
546 endosomes). Cellular and bacterial DNA was stained with DAPI. Boxed areas are magnified by
547 four-fold to show micrographs of indicated channels and representative GcAVs (white puncta).
548 Scale bars, 20 μ m. **f, g**, Representative fluorescent micrographs (**f**) and quantitation (**g**) of wild-
549 type HeLa/GFP-LC3 cells and HeLa *SNX5*^{KO}/GFP-LC3 cells undergoing non-canonical
550 autophagy after being cultured in either normal medium or hypotonic medium for 1 h. Boxed
551 areas are magnified by two-fold to show micrographs of individual channels. Scale bars, 20 μ m.
552 **h, i**, Representative differential interference contrast (DIC) microscopy and fluorescence
553 microscopy micrographs (**h**) and quantitation (**i**) of monensin-driven LC3-associated
554 phagocytosis (LAP) of latex beads in wild-type HeLa/GFP-LC3 cells and HeLa *SNX5*^{KO}/GFP-
555 LC3 cells that were treated with monensin (100 μ M) and polybead microspheres (3 μ m in
556 diameter) for 1 h. Boxed areas are magnified by nine-fold to show micrographs of DIC channel
557 and GFP channel. Scale bars, 20 μ m. In **b, c, e, g** and **i**, bars represent mean \pm s.d. of triplicate
558 samples (100-150 cells analyzed per sample). *P*-values were determined with one-way ANOVA
559 with Dunnett's test for multiple comparisons (**b** and **c**) or unpaired two-tailed *t*-test (**e, g** and **i**).
560 For **a, d, f**, and **h**, similar results were observed in three independent experiments.

561

562 **Extended Data Fig. 5. SNX5 is not required for retromer function and endolysosomal**
563 **function in HeLa cells.** **a, b**, Representative fluorescent micrographs (**a**) and quantitation (**b**) of
564 GLUT1 colocalized with the lysosomal marker LAMP1 in HeLa cells treated with indicated
565 siRNA (72 h). Colocalized GLUT1 and LAMP1 puncta (yellow) represent lysosomal
566 localization of mis-sorted GLUT1 which increases when retromer function is defective. Scale

567 bars, 20 μm . Bars in **b** represent mean \pm s.d. of Manders' overlap coefficient of GLUT1 and
568 LAMP1 of four replicates. **c-f**, Confirmation of gene knockdown in indicated siRNA-treated
569 HeLa cells (72 h) for experiments shown in **a** and **b** by western blot analyses of indicated
570 proteins (**c-e**) or quantitative real-time PCR of *SNX32* (**f**). Bars in **f** represent mean \pm s.d. of
571 triplicate samples. Similar results were observed in three independent experiments. **g**, Western
572 blot detection of SNX5 and actin in HeLa *SNX5*^{KO} cells and parental wild-type (WT) HeLa cells.
573 **h, i**, Quantitation of remaining protein levels of internalized plasma membrane-anchored
574 transferrin receptor (TfnR) in WT and *SNX5*^{KO} HeLa cells during fast (**h**) and slow (**i**) endocytic
575 recycling processes. **j, k**, Representative western blot analysis (**j**) and densitometry analysis (**k**)
576 of epidermal growth factor receptor (EGFR) and actin in WT and *SNX5*^{KO} HeLa cells at
577 indicated chase time after treating with EGF (100 ng/mL). Symbols in **h, i** and **k** represent mean
578 \pm s.d. of three independent experiments. *P*-values were determined with one-way ANOVA with
579 Dunnett's test for multiple comparisons (**b**), unpaired two-tailed *t*-test (**f**) or repeated measures
580 ANOVA (**h, i** and **k**). For **a, c-e, g**, and **j**, similar results were observed in three independent
581 experiments. For gel source data, see Supplementary Fig. 1.

582

583 **Extended Data Fig. 6. SNX5 restricts viral infection in HeLa cells and primary mouse**
584 **embryonic fibroblasts (MEFs) via an autophagy-dependent mechanism. a-d**, Viral
585 infectivity assay in WT and *SNX5*^{KO} HeLa cells infected with indicated virus. **e-h**, Viral multi-
586 step growth curves (MOI = 0.01) of WT and *SNX5*^{KO} HeLa cells infected with indicated virus. **i-**
587 **l**, Viral multi-step growth curves (MOI = 0.01) of *Snx5*^{+/+} and *Snx5*^{-/-} primary MEFs infected
588 with indicated virus. **m, n**, Viral infectivity assay in WT and *SNX5*^{KO} HeLa cells infected with
589 autophagy-suppressive viral strains, SIN.dnAtg5 and HSV-1 Δ BBD-MR. **o-r**, Viral multi-step

590 growth curves (MOI = 0.01) of WT and *SNX5*^{KO} HeLa cells (**o**, **p**) and *Snx5*^{+/+} and *Snx5*^{-/-}
591 primary MEFs (**q**, **r**) infected with SIN.dnAtg5 (**o**, **q**) and HSV-1ΔBBD-MR (**p**, **r**). In **a-d**, **m**
592 and **n**, bars represent mean ± s.d. of the number of viral plaques formed in cell monolayers of
593 three replicates. In **e-l** and **o-r**, symbols represent mean ± s.d. of viral titer of three replicates. **s**, **t**,
594 Viral entry efficiency in WT and *SNX5*^{KO} HeLa cells that were infected with SIN (MOI = 50) or
595 HSV-1ΔBBD (MOI = 25). Bars in **s** and **t** represent mean ± s.d. of SIN minus-strand RNA levels
596 (**s**) and HSV-1 immediate early gene *ICP27* mRNA levels (**t**) of triplicate samples at indicated
597 time point, respectively. **u**, **v**, Quantitative real-time PCR analyses of relative mRNA levels of
598 interferon beta (*IFN-β*; **u**) and the interferon-stimulated gene (ISG) interferon induced protein
599 with tetratricopeptide repeats 1 (*IFIT1*; **v**) in WT and *SNX5*^{KO} HeLa cells that were mock-
600 infected or infected with SIN or HSV-1ΔBBD (MOI = 10 and 5, respectively; 4.5 h). **w**,
601 Quantitative real-time PCR analyses of relative mRNA levels of *SNX5* in WT HeLa cells that
602 were infected similarly as in **u** and **v**. In **u-w**, bars represent mean ± s.d. of three replicates. *P*-
603 values were determined with unpaired two-tailed *t*-test (**a-d**, **m**, **n**, **s** and **t**), repeated measures
604 ANOVA (**e-l** and **o-r**) or one-way ANOVA with Dunnett's test for multiple comparisons (**u-w**).
605 Similar results were observed in three independent experiments.

606

607 **Extended Data Fig. 7. CNS viral titers, neuronal cell death and animal survival of virally-**
608 **infected *Snx5*^{+/+} and *Snx5*^{-/-} littermate mice.** **a-c**, CNS viral titers (**a**) and neuronal cell death
609 (**b**, **c**) in seven-day-old *Snx5*^{+/+} (n = 8) and *Snx5*^{-/-} (n = 8) littermate mice at indicated time point
610 after infection via intracerebral (i.c.) inoculation with SIN strain dsTE12Q (1,000 pfu/mouse). **d-**
611 **f**, CNS viral titers (**d**) and neuronal cell death (**e**, **f**) in eight- to ten-week-old *Snx5*^{+/+} (n = 8) and
612 *Snx5*^{-/-} (n = 8) littermate mice at indicated time point after infection via i.c. inoculation with

613 HSV-1 Δ BBD (50,000 pfu/mouse). In **b** and **e**, shown are representative micrographs of TUNEL
614 staining of mouse brain sections from cerebral cortex (**b**) or basal ganglia (**e**) at indicated time
615 point. Scale bars, 100 μ m. Arrowheads denote representative TUNEL-positive foci that would be
616 scored as positive in **c** and **f**. In **a**, **c**, **d** and **f**, each data point represents an individual mouse and
617 black horizontal lines represent median values. **g**, Kaplan-Meier survival curve of eight- to ten-
618 week-old *Snx5*^{+/+} and *Snx5*^{-/-} littermate mice infected i.c. with the autophagy-suppressive strain
619 HSV-1 Δ BBD-MR (500 pfu/mouse). Results represent combined survival data for three
620 independent infection experiments. Similar results were observed in each independent infection.
621 *P*-values were determined with unpaired two-tailed *t*-test (**a**, **c**, **d** and **f**) or two-sided log-rank
622 test (**g**).

623

624 **Extended Data Fig. 8. Autophagy inhibition by PIK-III in baseline conditions, starvation**
625 **and mTOR inhibition; western blot analysis of bacterially-purified SNX5 proteins; and**
626 **bioinformatic analyses of SNX5 amino-acid sequences (related to Fig. 2).** **a-c**, Representative
627 western blots (**a**) and densitometry analyses (**b**, **c**) of indicated proteins in WT HeLa cells
628 cultured in normal media in the presence or absence of PIK-III (5 μ M) for 1 h. Bars in **b** and **c**
629 represent mean \pm s.d. of total LC3/actin ratios (**b**) and p62/actin ratios (**c**) of three replicates. **d**, **e**,
630 Representative fluorescent micrographs (**d**) and quantitation (**e**) of GFP-LC3 puncta in
631 HeLa/GFP-LC3 cells that were cultured in normal medium (1 h), starvation medium (EBSS; 1
632 h), or normal medium containing torin 1 (250 nM; 1 h) in the presence or absence of PIK-III (5
633 μ M; 1 h) and Baf A1 (100 nM; 1h). Scale bars, 20 μ m. Arrows denote representative
634 autophagosomes that would be scored as positive in **e**. Bars in **e** represent mean \pm s.d. of three
635 replicates (100-150 cells analyzed per sample). In **b**, **c** and **e**, unpaired two-tailed *t*-test was used

636 to compare means of PIK-III- versus DMSO-treated cells. In **e**, one-way ANOVA with
637 Dunnett's test for multiple comparisons was used to compare means of starvation or torin 1
638 treatment versus normal condition. **f**, Western blot analysis of His-tagged SUMO, SUMO-SNX5
639 or SUMO-SNX5 EEE that were used in the experiments shown in Fig. 2c-i. For gel source data,
640 see Supplementary Fig. 1. For **a**, **d**, and **f**, similar results were observed in three independent
641 experiments. **g**, Amino acid sequence alignment of human SNX5 amino acids 298-361 (within
642 the BAR domain) with the homologous regions of Snx5 proteins from eight other vertebrate
643 animals using Cluster Omega (<https://www.ebi.ac.uk/Tools/msa/clustalo/>). Grey box highlights a
644 highly conserved region across nine vertebrate SNX5 homologs. **h**, Amino acid sequence
645 alignment of human retromer-related sorting nexins. Black arrowheads denote three positively
646 charged residues (K429, K430 and R431) in human SNX1 for which triple mutations to glutamic
647 acid residues (SNX1 EEE) lead to the inability of SNX1 to associate to membranes and induce
648 membrane remodeling³³. In **g** and **h**, red dots indicate the residues of a positively charged stretch
649 (K328, R330 and K332) in human SNX5 that corresponds to amino acids K429, K430, and R431
650 in SNX1. The three residues in SNX5 (K328, R330 and K332) were substituted with glutamic
651 acid residues to generate the SNX5 EEE mutant used in this study. Hyphens (-) denote gaps in
652 the indicated sequence identified by sequence alignment. Asterisks (*) indicate positions with a
653 fully conserved residue; colons (:) indicate conserved positions between groups of strongly
654 similar properties (scoring > 0.5 in the Gonnet PAM 250 matrix); periods (.) indicate conserved
655 positions between groups of weakly similar properties (scoring equal to or < 0.5 in the Gonnet
656 PAM 250 matrix). Magenta cylinders represent predicted discontinued alpha helices using the
657 University College London (UCL) PSIPRED Protein Sequence Analysis Workbench

658 (<http://bioinf.cs.ucl.ac.uk/psipred/>). Solid line indicates a turn conformation in the tip region of
659 the SNX1 and SNX5 BAR domains³⁸.

660

661 **Extended Data Fig. 9. SNX5 is required for formation of PI3P probe puncta and WIPI2**
662 **puncta during viral infection, but not in baseline conditions, or upon autophagy induction**
663 **by starvation or mTOR inhibition. a-d**, Representative fluorescent micrographs (**a**, **c**) and
664 quantitation (**b**, **d**) of PI3P probe staining (**a**, **b**) or WIPI2 immunostaining (**c**, **d**) in indicated
665 HeLa cells that were either mock-infected or infected with SIN or HSV-1 Δ BBD (MOI = 10 and
666 5, respectively; 4 h). **e-h**, Representative fluorescent micrographs (**e**, **g**) and quantitation (**f**, **h**) of
667 PI3P probe staining (**e**, **f**) or WIPI2 immunostaining (**g**, **h**) in indicated HeLa cells cultured in
668 normal medium (1 h), starvation medium (EBSS; 1 h), or normal medium containing torin 1 (250
669 nM; 1 h). Scale bars, 20 μ m. In **a**, **c**, **e** and **g**, arrows denote representative PI3P probe puncta or
670 WIPI2 puncta that would be scored as positive in **b**, **d**, **f** and **h**. In **c** and **g**, representative cells are
671 outlined by dashed white lines and boxed areas are magnified by sixteen-fold in the insets. In **b**,
672 **d**, **f** and **h**, bars represent mean \pm s.d. of three replicates (100-150 cells analyzed per sample). In
673 **b**, **d**, **f** and **h**, *P*-values were determined by one-way ANOVA with Dunnett's test for multiple
674 comparisons. **i**, Western blot analyses of SNX5 and actin in parental wild-type HeLa cells (WT)
675 and HeLa *SNX5*^{KO} cells (KO) reconstituted with either empty vector (WT + vector and KO +
676 vector), wild-type SNX5 (KO + SNX5) or SNX5 EEE mutant (KO + SNX5 EEE). For **a**, **c**, **e**, **g**,
677 and **i**, similar results were observed in three independent experiments. For gel source data, see
678 Supplementary Fig. 1.

679

680 **Extended Data Fig. 10. SNX5 is not required for virus-induced endosomal localization of**
681 **PI3KC3-C1 complexes, and PI3KC3 is required for virus-induced formation of PI3P probe**
682 **puncta and WIPI2 puncta in HeLa cells. a**, Representative fluorescent micrographs of
683 indicated immunostaining in parental wild-type and *SNX5*^{KO} HeLa cells that were either mock-
684 infected or infected with SIN and HSV-1ΔBBD (MOI = 10 and 5, respectively; 2 h). Scale bars,
685 20 μm. Boxed areas are magnified by four-fold in the insets. **b-e**, Representative fluorescent
686 micrographs (**b** and **d**) and quantitation (**c** and **e**) of PI3P probe staining (**b**, **c**) or WIPI2
687 immunostaining (**d**, **e**) in HeLa cells that were either mock-infected or infected with SIN or
688 HSV-1ΔBBD (MOI = 10 and 5, respectively; 4 h) and treated for 1 h with PIK-III (5 μM) or
689 DMSO control prior to fixation (from 3 hpi to 4 hpi). Scale bars, 20 μm. Arrows in **b** and **d**
690 denote representative PI3P probe puncta and WIPI2 puncta that would be scored as positive in **c**
691 and **e**, respectively. In **d**, representative cells are outlined by dashed white lines and boxed areas
692 are magnified by sixteen-fold in the insets. Bars in **c** and **e** represent mean ± s.d. of three
693 replicates (100-150 cells analyzed per sample). In **c** and **e**, unpaired two-tailed *t*-test was used to
694 compare means of PIK-III- versus DMSO-treated cells, and one-way ANOVA with Dunnett's
695 test for multiple comparisons was used to compare means of SIN or HSV-1ΔBBD infection
696 versus mock infection. For **a**, **b**, and **d**, similar results were observed in three independent
697 experiments.

698

699 **Methods**

700 ***Mammalian cell lines and cell culture***

701 All cell culture reagents including media, sera, antibiotics and trypsin-EDTA (0.25%), were
702 purchased from Invitrogen/Gibco (Thermo Fisher Scientific) unless otherwise specified. Primary
703 mouse embryonic fibroblasts (MEFs) were isolated from *Snx5*^{+/+} and *Snx5*^{-/-} littermate offspring
704 on embryonic day (E) 13.5 as previously described³⁹. HeLa, BHK-21, Vero and 293T cell lines
705 were obtained from American Type Culture Collection (ATCC), which have been thoroughly
706 tested and authenticated by ATCC. Additional authentication of HeLa cells was performed by
707 the ATCC Cell Line Authentication Service using short-tandem repeat profiling (STR) analysis.
708 Vero E6 cell line was a gift from Matthew B. Frieman (University of Maryland), which
709 originally sourced from ATCC (CRL-1586) and was not further authenticated. MDCK cell line
710 was a gift from Charles M. Rice (The Rockefeller University), which was authenticated as canine
711 origin by cloning and sequencing immune genes from stimulated cells. HEK293F cell line was a
712 gift from Hongwei Wang (Tsinghua University). All the cell lines used in this study tested
713 negative for mycoplasma contamination using PCR-based Venor GeM Mycoplasma Detection
714 Kit (Sigma-Aldrich MP0025). All the cell lines were cultured and maintained according to
715 ATCC's instructions, and used at low passage numbers. HeLa cell clones were cultured in Opti-
716 MEM I Reduced Serum Medium supplemented with 5% fetal bovine serum (FBS), 100 units/mL
717 penicillin and 100 µg/mL streptomycin. MEFs, BHK-21 cells, Vero cells, Vero E6 cells, MDCK
718 cells and HEK293T cells were cultured in Dulbecco's Modified Eagle Medium (DMEM)
719 supplemented with 10% FBS, 100 units/mL penicillin and 100 µg/mL streptomycin. Media
720 supplemented with heat-inactivated (HI) FBS were used for viral infection experiments.
721 HEK293F cells were cultured in SMM293-TI medium (Sino Biological) supplemented with 100

722 units/mL penicillin and 100 µg/mL streptomycin. HeLa/GFP-LC3 cells that stably express GFP-
723 LC3 were generated by transfecting HeLa cells with a plasmid pIRES.GFP-LC3.neo3 and
724 selection in medium containing 500 ng/mL geneticin. HeLa *SNX5* CRISPR knockout cell lines
725 (HeLa *SNX5*^{KO}) were generated by CRISPR/Cas9-induced double-strand break at the Genome
726 Engineering and iPSC Center (GEiC) of Washington University School of Medicine (St. Louis,
727 MO). Sequences encompassing candidate guide RNA (gRNA) sites were analyzed for common
728 (>1%) single nucleotide polymorphisms (SNPs) using the UCSC Genome Browser
729 (<https://genome.ucsc.edu>), and no common SNPs were detected in the selected two gRNAs for
730 the target gene. The sequences of gRNAs used for CRISPR knockout are as follows: *SNX5*
731 exon5.g7: 5'-CCGCTGAAGAAAGACTTCATNGG-3' and *SNX5* exon5.g8: 5'-
732 CTGAAGAAAGACTTCATGGGNGG-3'. Frequencies of local insertions and deletions (indels)
733 in a *SNX5* CRISPR knockout clone were determined using targeted deep sequencing, which
734 confirmed the gRNA-targeted *SNX5* deletion in the HeLa cell genome. Reconstituted HeLa
735 *SNX5*^{KO}/*SNX5* cells, HeLa *SNX5*^{KO}/*SNX5* EEE cells, HeLa *SNX5*^{KO}/vector cells, and HeLa
736 WT/vector control cells were generated by infection with retroviruses expressing wild-type
737 human *SNX5*, *SNX5* EEE mutant (K328E/R330E/K332E; Extended Data Fig. 8g, h), or an
738 empty vector, which was followed by selection in medium containing 500 ng/mL puromycin.
739 HeLa *SNX5*^{KO}/GFP-LC3 cells were generated by transfecting HeLa *SNX5*^{KO} cells with a plasmid
740 pIRES.GFP-LC3.neo3 and selection in medium containing 500 ng/mL geneticin. Reconstituted
741 HeLa *SNX5*^{KO}/GFP-LC3/*SNX5* cells were generated by transfecting HeLa *SNX5*^{KO}/GFP-LC3
742 cells with a plasmid pIRES.*SNX5*.puro3 and selection in medium containing 500 ng/mL
743 puromycin. For viral infection experiments using the stable cell lines described above, selection

744 antibiotics (such as geneticin or puromycin) were withdrawn from the culture media for at least
745 24 h prior to viral infection.

746 ***Mouse strains***

747 C57BL/6J mice were obtained from The Jackson Laboratory and all mouse strains used in this
748 study were backcrossed to female C57BL/6J breeders for more than ten generations. *Snx5*^{-/-} mice
749 were generated by the UC DAVIS Knockout Mouse Project (KOMP) Repository
750 (<https://www.komp.org/>) and have been previously described²³. Genomic DNA from mice was
751 prepared from mouse tail using DirectPCR Lysis Reagent (Viagen Biotech) and Proteinase K
752 (Roche). Mouse genotypes were determined by PCR using TaKaRa SapphireAmp Fast PCR
753 Master Mix (Clontech) and the following primer pairs: *Snx5* WT-1, 5'-
754 GCTTTGCCTCTGATTTGGATCTCC-3'; *Snx5* WT-2, 5'-
755 CTAAGACAATAAAACCCACCGGGCG-3'; *Snx5* KO-1, 5'-
756 GACATGAGCACACTGTTAGTGCAGG-3'; *Snx5* KO-2, 5'-
757 GAGATGGCGCAACGCAATTAATG-3'. The PCR conditions are as follows: 1 min at 94°C, 35
758 cycles of amplification stage (5 sec at 98°C, 5 sec at 55°C and 5 sec at 72°C) and 5 min at 72°C.
759 *Snx5*^{+/+} genomic DNA yields a 405-bp band; *Snx5*^{-/-} genomic DNA yields a 386-bp band; *Snx5*^{+/-}
760 genomic DNA yields both a 405-bp band and a 386-bp band.

761 ***Chemicals***

762 Bafilomycin A1 (Baf A1; Sigma-Aldrich B1793), a lysosomal inhibitor, was dissolved in sterile-
763 filtered DMSO (Sigma-Aldrich D2650) as a 100 µM stock solution. Cycloheximide (Sigma-
764 Aldrich C7698) was dissolved in sterile water as a 10 mg/mL stock solution and then passed
765 through a 0.22-µm filter. Monensin (Sigma-Aldrich M5273) was dissolved in ethanol (Thermo
766 Fisher Scientific) as a 50 mg/mL (72.2 mM) stock solution. PIK-III (Selleck Chemicals S7683),

767 a PI3KC3 (VPS34)-specific inhibitor⁴⁰, was dissolved in sterile-filtered DMSO as a 4 mM stock
768 solution. Torin 1 (Selleck Chemicals S2827), an mTOR inhibitor⁴¹, was dissolved in sterile-
769 filtered DMSO as a 1 mM stock solution. All stock solutions were stored in small aliquots at -
770 20°C. For control groups of chemical treatment, equivalent volume of according chemical-free
771 sterile solvent was added into culture media.

772 ***Antibodies***

773 The following commercial antibodies (vendor, catalog number and dilution) were used for
774 immunoprecipitation, western blot analyses and immunofluorescence staining according to
775 manufacturers' instructions: mouse anti-actin monoclonal antibody (Sigma-Aldrich A1978,
776 1:1000), mouse anti-actin monoclonal antibody (C4) HRP (Santa Cruz Biotechnology sc-47778
777 HRP, 1:5000), rabbit anti-ATG7 polyclonal antibody (Sigma-Aldrich A2856, 1:1000), rabbit
778 anti-ATG13 monoclonal antibody (Abcam ab201467, 1:2000), mouse anti-ATG14 monoclonal
779 antibody (MBL International Corporation M184-3, 1:500 for western blot and 1:1000 for
780 immunofluorescence staining), rabbit anti-ATG14 polyclonal antibody (Cell Signaling
781 Technology 5504S, 1:500), mouse anti-beclin 1 monoclonal antibody (E-8) (Santa Cruz
782 Biotechnology sc-48341, 1:1000 for western blot and 1:100 for immunoprecipitation), rabbit
783 anti-beclin 1 polyclonal antibody (H-300) (Santa Cruz Biotechnology sc-11427, 1:1000), goat
784 anti-EEA1 polyclonal antibody (N-19) (Santa Cruz Biotechnology sc-6415, 1:200), rabbit anti-
785 EEA1 polyclonal antibody (H-300) (Santa Cruz Biotechnology sc-33585, 1:200), rabbit anti-
786 EGFR monoclonal antibody (Cell Signaling Technology 4267S, 1:1000), rabbit anti-GLUT1
787 polyclonal antibody (Abcam ab15309, 1:500), mouse 6×-His tag monoclonal antibody (HIS.H8)
788 (Thermo Fisher Scientific MA1-21315, 1:500), goat anti-LAMP1 polyclonal antibody (C-20)
789 (Santa Cruz Biotechnology sc-8098, 1:200), rabbit anti-LC3B polyclonal antibody (Novus

790 Biologicals NB100-2220, 1:2000), guinea pig anti-p62/SQSTM1 (C-terminus) polyclonal serum
791 (Progen GP62-C, 1:1000), mouse anti-p62/SQSTM1 monoclonal antibody (Abnova H00008878-
792 M01, 1:5000), goat anti-SNX5 polyclonal antibody (Abcam ab5983, 1:100 for both
793 immunoprecipitation and western blot), mouse anti-SNX5 monoclonal antibody (F-11) (Santa
794 Cruz Biotechnology sc-515215, 1:400 for western blot and 1:200 for immunofluorescence
795 staining), rabbit anti-UVRAG monoclonal antibody (D2Q1Z) (Cell Signaling Technology
796 13115, 1:500), rabbit anti-UVRAG polyclonal antibody (Sigma-Aldrich U7508, 1:1000), rabbit
797 anti-VPS29 polyclonal antibody (Abcam ab98929, 1:500), rabbit anti-VPS34 monoclonal
798 antibody (D9A5) (Cell Signaling Technology 4263S, 1:100 for western blot and 1:200 for
799 immunofluorescence staining), mouse anti-WIPI2 monoclonal antibody (Bio-Rad Laboratories
800 MCA5780GA, 1:200), normal goat IgG (Abcam ab37373, 1:1000), normal mouse IgG (Santa
801 Cruz Biotechnology sc-2025, 1:200), donkey anti-goat IgG-HRP (Santa Cruz Biotechnology sc-
802 2056, 1:1000), goat anti-guinea pig IgG H&L (HRP) (Abcam ab6908, 1:2000), peroxidase
803 AffiniPure goat anti-mouse IgG Fc γ fragment specific antibody (Jackson ImmunoResearch
804 Laboratories 115-035-071, 1:2000), donkey anti-rabbit IgG HRP-conjugate species-adsorbed
805 (EMD Millipore AP182P, 1:2000), donkey anti-goat IgG (H+L) cross-adsorbed secondary
806 antibody Alexa Fluor 594 (Thermo Fisher Scientific A11058, 1:1000), donkey anti-goat IgG
807 (H+L) cross-adsorbed secondary antibody Alexa Fluor 647 (Thermo Fisher Scientific A-21447,
808 1:1000), donkey anti-mouse IgG (H+L) highly cross-adsorbed secondary antibody Alexa Fluor
809 488 (Thermo Fisher Scientific A21202, 1:1000), donkey anti-rabbit IgG (H+L) highly cross-
810 adsorbed secondary antibody Alexa Fluor 488 (Thermo Fisher Scientific A-21206, 1:1000), and
811 donkey anti-rabbit IgG (H+L) highly cross-adsorbed secondary antibody Alexa Fluor 594
812 (Thermo Fisher Scientific A21207, 1:1000).

813 ***Bacteria***

814 *Streptococcus pyogenes* (also known as Group A *Streptococcus*) wild-type serotype M6 strain
815 JRS4 (M6⁺F1⁺) and the isogenic mutant JRS4ΔSLO were kindly provided by Ichiro Nakagawa
816 (Kyoto University)¹⁹. JRS4ΔSLO lacks the gene streptolysin O (*SLO*), a cholesterol-dependent
817 pore-forming exotoxin, and thus does not escape from endosomes and induce Group A
818 *Streptococcus*-containing autophagosome-like vacuoles (GcAVs) in HeLa cells¹⁹. Group A
819 *Streptococcus* strains were amplified in BBL Brain Heart Infusion medium (Becton, Dickinson
820 and Company) in a 5% CO₂ incubator. For subcloning, Invitrogen MAX Efficiency DH5α
821 Competent Cells (Thermo Fisher Scientific) were transformed with plasmids and selected on LB
822 agar plates with certain selection antibiotics. Isolated single colonies were cultured in Difco
823 Terrific Broth medium (Becton, Dickinson and Company) in an Innova 43 Incubator Shaker
824 (New Brunswick Scientific). Bacterial plasmids for cloning experiments were amplified using a
825 Plasmid Midi Kit (QIAGEN) and stored in -20°C. The insertion fragment in a plasmid was
826 confirmed by Sanger sequencing.

827 ***Viral strains***

828 A herpes simplex virus type 1 (HSV-1) mutant strain (HSV-1ΔBBD) was previously genetically
829 engineered to express a neurovirulent factor ICP34.5 mutant that lacks the beclin 1-binding
830 domain (BBD) and is unable to suppress autophagy^{5,42}. A marker-rescued HSV-1 control strain
831 (HSV-1ΔBBD-MR) expressing wild-type ICP34.5 was generated in parallel and shown to
832 suppress autophagy in both cultured neuronal cells and brains of intracerebrally infected mice⁵.
833 The Sindbis virus (SIN) strain SVIA (ATCC) was derived from a low-passage isolate of the
834 wild-type SIN strain AR339⁴³. In this study, the SIN strain used in the majority of cell culture
835 infection experiments was SVIA unless otherwise specified. The recombinant SIN strain with a

836 double subgenomic promoter generated from the SIN vector, dsTE12Q, was previously
837 described⁴⁴, as was the recombinant SIN strain dsTE12Q.dnAtg5 (SIN.dnAtg5), which expresses
838 a dominant negative mutant of autophagy core machinery protein, Atg5 K130R, from the second
839 subgenomic promoter, and has been previously shown to inhibit autophagy in brains of
840 intracerebrally infected mice⁶. Recombinant SIN strains, SIN.dnAtg5 and its parental wild-type
841 control dsTE12Q, were used in animal experiments (Fig. 1c, Extended Data Fig. 7a-c) and some
842 *in vitro* experiments (Extended Data Fig. 6m, o, q). The recombinant SIN strain SIN.mCherry-E2
843 that express mCherry-fused envelope glycoprotein E2 was previously described³⁵. The following
844 additional viral strains were used in this study: chikungunya virus (CHIKV) strain 06-021⁴⁵ (a
845 gift from Deborah J. Lenschow, Washington University); Coxsackievirus B3 strain H3 (CVB3-
846 H3) generated from an infectious clone (a gift from Marco Vignuzzi, Pasteur Institute); influenza
847 A virus (IAV) strain A/WSN/33 (a gift from Adolfo Garcia-Sastre, Icahn School of Medicine at
848 Mount Sinai); poliovirus generated from the Mahoney type 1 infectious clone (a gift from Karla
849 Kirkegaard, Stanford University); West Nile virus (WNV) strain TX02⁴⁶ (a gift from Michael
850 Gale Jr., University of Washington) for infection of HeLa cells and MEFs; WNV strain Egypt-
851 101⁴⁷ (a gift from Michael S. Diamond, Washington University) for mouse infection; and Zika
852 virus strain MR-766 (obtained from Centers for Disease Control and Prevention [CDC]). Viral
853 stocks were propagated and titrated by plaque assays in Vero cells (for HSV-1 and CHIKV),
854 BHK-21 cells (for SIN and WNV), Vero E6 cells (for Zika virus), HeLa cells (for poliovirus and
855 CVB3) and MDCK cells (for IAV), respectively.

856 ***Retroviruses for reconstitution of HeLa SNX5^{KO} cell lines***

857 To generate reconstituted HeLa SNX5^{KO} cell lines, retroviruses were constructed by co-
858 transfection of HEK293T cells with pCMV-VSV-G (Addgene plasmid #8454), pUMVC

859 (Addgene plasmid #8449), and pBABE-puro empty vector (Addgene plasmid #1764), pBABE-
860 puro-Flag-SNX5 or pBABE-puro-Flag-SNX5 EEE (that carries K328E/R330E/K332E triple
861 mutations) at a mass ratio of 1:9:10 according to Addgene's instructions. Cell culture
862 supernatants were collected at 48 h and 72 h post transfection. Combined supernatants were pre-
863 cleared by centrifugation at 1,000 g and 4°C for 15 min and then passed through sterilized 0.45-
864 µm filters (EMD Millipore). Target cells were infected with fresh media containing retroviral
865 supernatants and 8 µg/mL polybrene (Santa Cruz Biotechnology sc-134220) for 5 h. Retrovirus-
866 containing media were then replaced with fresh virus-free medium, cultured for an additional 48
867 h, and cells were selected in medium containing 500 ng/mL puromycin.

868 ***Small interfering RNAs (siRNAs)***

869 All siRNA oligonucleotides used in this study were synthesized by Dharmacon. The high-
870 content siRNA screens used a genome-wide human siRNA library (siGENOME of Dharmacon)
871 containing 18,115 SMARTpools, in which each pool contains four siRNA oligonucleotides
872 targeting an individual gene. The sequences or catalog number of non-targeting control siRNAs
873 (NC) and gene-specific siRNA oligonucleotides are as follows: NC, 5'-
874 AUCCGCGCGAUAGUACGUA-3' and 5'-UUACGCGUAGCGUAAUACG-3'; *ATG7*, 5'-
875 GGGUUAUUACUACAAUGGUG-3'; *ATG13*, 5'-AGACCAUCUUUGUCCGAAA-3' and 5'-
876 GAAGAAUGUCCGCGAGUUU-3'; *SNX5*, siGENOME siRNA D-012524-01, D-012524-02,
877 D-012524-03 and D-012524-04; *SNX32*, ON-TARGETplus SMARTpool L-017082-01; *VPS29*,
878 ON-TARGETplus SMARTpool L-009764-01.

879 ***High-content image-based genome-wide siRNA screens***

880 *Primary screens:* The siGENOME library siRNA pools were seeded in parallel into nine
881 identical SensiPlate glass-bottom 96-well microplates (Greiner Bio-One 655892) in 25 µL Opti-

882 MEM I Reduced Serum Medium at a final concentration of 50 nM using a BioMek FX Robotic
883 Liquid Handling System (Beckman Coulter Life Sciences), followed by addition of Invitrogen
884 Lipofectamine RNAiMAX (Thermo Fisher Scientific) in 25 μ L Opti-MEM I Reduced Serum
885 Medium at a final dilution of 1:500 with an EL406 Washer Dispenser (BioTek Instruments).
886 siRNA oligonucleotides were incubated with Lipofectamine RNAiMAX for 30 min at room
887 temperature, followed by addition of 6,000 HeLa/GFP-LC3 cells in 100 μ L Opti-MEM I
888 Reduced Serum Medium supplemented with 5% HI FBS, 100 units/mL penicillin and 100
889 μ g/mL streptomycin (normal medium) using a Multidrop 96/384 Microplate Dispenser (MTX
890 Lab Systems) for reverse transfection. For all the 96-well plates, the first column and the twelfth
891 column were used for on-plate negative and positive controls, which contained alternating wells
892 of non-targeting control siRNAs (NC) and siRNA targeting the essential autophagy gene *ATG7*;
893 and column 2 to column 11 contained siGENOME library siRNA pools (one well/plate/pool).
894 Three sets of triplicate plates (Plate 1 to Plate 3, Plate 4 to Plate 6, and Plate 7 to Plate 9) were
895 used for mock infection, SIN infection and HSV-1 Δ BBD infection, respectively. After 48-hour
896 siRNA knockdown, Plate 1 to Plate 3 were mock-infected by dispensing 40 μ L/well of virus-free
897 normal medium using an EL406 Washer Dispenser. For the two sets of triplicate plates used for
898 viral infection, the first columns of Plate 4 to Plate 9 were mock-infected by dispensing 40
899 μ L/well of virus-free normal medium (on-plate mock infection controls), and column 2 to
900 column 12 of these plates were infected by dispensing 40 μ L/well of normal media containing
901 SIN strain SVIA (at a multiplicity of infection [MOI] of 10) or HSV-1 Δ BBD (MOI = 5),
902 respectively. After 1.5-hour incubation at 37 $^{\circ}$ C (viral adsorption and entry), the culture media in
903 all nine plates were replaced with 200 μ L/well of fresh normal medium using an EL406 Washer
904 Dispenser. After an additional 2.5-hour incubation at 37 $^{\circ}$ C, 25 μ L normal medium containing

905 Invitrogen Hoechst 33342 (Thermo Fisher Scientific) was added to each well (at a final
906 concentration of 5 $\mu\text{g}/\text{mL}$) to stain cellular nuclei. After 20-min additional incubation at 37°C
907 (approximately 4.5 hours post infection [hpi]), medium was aspirated using an EL406 Washer
908 Dispenser and all plates were immediately fixed with 100 μL pre-warmed 3% paraformaldehyde
909 (PFA) (Electron Microscopy Sciences) in 1× Gibco PBS containing Ca^{2+} and Mg^{2+} (Thermo
910 Fisher Scientific) for 20 min at room temperature. The fixation solution was replaced with 1×
911 Gibco PBS (Thermo Fisher Scientific), and all plates were sealed with Microplate Aluminum
912 Tapes (Corning) and stored at 4°C until imaging. All assay plates were imaged within three days
913 after fixation.

914 *High-content automated imaging:* Digital images were acquired with a BD Pathway 855
915 Bioimaging System (BD Biosciences) using an Olympus UAPO/340 40× 340nm air objective
916 (0.9 NA). The microscope filters used for imaging were: Hoechst channel (Ex: 360/10, Dichroic:
917 400DCLP, Em: 435LP), GFP channel (Ex: 488/10, Dichroic: Fura/FITC, Em: 515LP) and wide-
918 field epifluorescence. Raw micrographs of the Hoechst channel were utilized to determine cell
919 boundaries by a watershed segmentation method, which uses Hoechst-positive nuclei as markers
920 and cytosolic Hoechst signal as the background. After cell segmentation, raw micrographs of the
921 GFP channel were further analyzed to obtain numbers of subcellular GFP-LC3 puncta per cell
922 for each micrograph using the Imaging and Advanced Imaging packages in the software Pipeline
923 Pilot 8.5 (Accelrys). Approximately 250 to 450 cells were analyzed per well.

924 *Assessment of viral infection:* To determine whether siRNA knockdown indirectly affected
925 autophagy levels through inhibition of early stages of viral infection (e.g. attachment and
926 uptake), 316 candidate hits from the primary screens were further examined using the same
927 conditions as for the primary screens. Four cherry-picked siRNA library plates (96-well) were

928 generated using the 316 siRNA pools that scored positive in the primary screens. The assay
929 plates were prepared similarly as for the primary screens. Instead of PFA fixation at 4.5 hpi,
930 assay plates were immediately frozen after incubation with viral inoculum for 1.5 h (1.5 hpi) and
931 stored at -80°C for quantitation of viral loads by plaque assay titration (after three freeze-thaw
932 cycles).

933 *Deconvolution screens:* To rule out false-positive hits due to off-target effects of individual
934 siRNA oligonucleotides, 310 candidate genes that passed primary screens were further re-
935 screened for their efficacy in decreasing the number of GFP-LC3 puncta in HeLa/GFP-LC3 cells
936 infected with SIN and HSV-1ΔBBD. Sixteen customized Dharmacon siRNA library plates (96-
937 well) were generated with four siRNA oligonucleotides for each gene (one siRNA
938 oligonucleotide per well). A total of forty wells of NC oligonucleotide was added in the middle
939 of the plates (columns 2 to 11) which served as on-plate negative controls. The assay plates were
940 prepared similarly as for the primary screens, except that individual siRNA oligonucleotides
941 (instead of siRNA pools) were used for gene knockdown.

942 *Quality control (QC) of high-content siRNA screens:* Given that 2,268 assay plates (in 35
943 batches) were used throughout the primary and deconvolution screens, one sentinel assay plate
944 was included for each batch of experiment to monitor batch-to-batch variation. For these sentinel
945 assay plates, NC and siRNAs targeting *ATG7* (48 wells each) were seeded in an alternating
946 pattern on 96-well microplates. All sentinel assay plates were handled together with the set of
947 assay plates for mock infection using the same procedure. After image acquisition and
948 quantitation of numbers of GFP-LC3 puncta, the sensitivity and the specificity of the analysis
949 method was evaluated based on the true positive (*ATG7* siRNA) and true negative (negative
950 control siRNA) wells. The receiver operating characteristic (ROC) curves were plotted (e.g.

951 Extended Data Fig. 2e), and the areas under the curves (AUC) values were calculated to evaluate
952 the screening performance. The ROC mean \pm s.d. of all the QC plates was 0.97 ± 0.03 , which
953 indicates accuracy and specificity in the identification of cellular factors that regulate numbers of
954 GFP-LC3 puncta.

955 *Statistical analyses of siRNA screens:* In the primary siRNA screens, we applied three
956 filters: (1) absence of cytotoxicity of siRNA pools in transfected cells; (2) lack of effect of
957 siRNA pools on numbers of GFP-LC3 puncta in mock-infected cells (basal autophagy); and (3)
958 significant reduction of numbers of GFP-LC3 puncta in cells infected with either SIN or HSV-
959 1 Δ BBD (virus-induced autophagy). siRNA pools that have at least two out of three replicate
960 wells with cell numbers less than 100 per montage were considered to have cytotoxic effects in
961 transfected cells and excluded from statistical analyses. To identify siRNA pools that alter only
962 virus-induced autophagy but not basal autophagy, we then performed the following two
963 analyses:

964 The first analysis used a mixed-effects Poisson regression, where the number of GFP-LC3
965 puncta in each cell serves as the response variable and the siRNA treatment (using negative
966 control wells as references) serves as the independent variable. A random intercept was included
967 to model the correlated observations among cells within each well. This analysis was performed
968 independently for each of the three screens (mock infection, SIN infection and HSV-1 Δ BBD
969 infection) and for each of the triplicate plates of each screen. The coefficient value indicates the
970 magnitude of the effect of an siRNA treatment on numbers of GFP-LC3 puncta compared to that
971 of NC treatment, and the two-sided *P*-value from Wald-test indicates the statistical significance
972 of the effect. The siRNA pools with either coefficient values greater than $\log(1/2)$ (i.e. 50%
973 reduction) or *P*-values greater than 0.05 in at least two out of the three replicate mock infection

974 assay plates were considered as siRNA pools that do not suppress basal autophagy. The siRNA
975 pools with coefficient values less than $\log(1/2)$ and P -values less than 0.05 in at least two out of
976 the three replicate viral infection assay plates were considered as siRNA pools that suppress SIN-
977 induced autophagy and/or HSV-1 Δ BBD-induced autophagy. The siRNA pools that specifically
978 suppress virus-induced autophagy without suppressing basal autophagy were considered as
979 candidate hits in this analysis.

980 The second analysis also used a mixed-effects Poisson regression, where the number of
981 GFP-LC3 puncta in each cell serves as the response variable. Unlike the first analysis that
982 inspects each plate separately, this analysis used a single integrated model to analyze all nine
983 assay plates from three screens (mock infection, SIN infection and HSV-1 Δ BBD infection).
984 Random intercepts were used to take into account correlated observations among cells in the
985 same well or cells in different wells but in the same assay plate. In addition to the main effects of
986 siRNA treatment and viral infections, the fixed effects also included their interactions, the
987 coefficient values of which indicate the difference in the siRNA's effect during viral infections
988 compared to that during mock infection, and the two-sided P -values of the interaction terms from
989 Wald-test indicate the statistical significance of such difference. The siRNA pools with
990 coefficient values of the interaction term less than $\log(1/2)$ and P -values less than 0.05 were
991 considered as candidate hits in this analysis, whose effects on virus-induced autophagy are more
992 pronounced than on basal autophagy.

993 Both the first analysis and the second analysis described above were performed in open-
994 source R software (www.r-project.org) version 3.1.0 with package lme4 version 1.0-4. The
995 overlapping siRNA pools identified by both statistical analyses were considered as candidate
996 unique hits involved specifically in virus-induced autophagy. The first analysis ensured that

997 scored candidate siRNA pools significantly suppressed virus-induced autophagy at the desired
998 threshold magnitude while not suppressing basal autophagy. The second analysis further ensured
999 that scored candidate siRNA pools led to statistically significantly greater reduction of autophagy
1000 (i.e. GFP-LC3 puncta number) during viral infection than during mock infection.

1001 For assessing early stages of viral infection, the relative fold of viral load for each well of
1002 the 316 overlapping siRNA pools (that were identified as candidate hits by both statistical
1003 analyses) was normalized in reference to the median viral loads of NC-treated wells on the first
1004 and twelfth columns for each assay plate. For each well, normalized viral loads that were either
1005 less than 0.2 or larger than 5 were considered to represent a biologically significant effect, and
1006 siRNA pools that altered intracellular viral loads in at least two out of three wells were
1007 considered as siRNA pools that alter early stages of viral infection (and thereby indirectly affect
1008 virus-induced autophagy). Six such genes were removed from the candidate list from primary
1009 screens: *ZNF224* (Entrez Gene ID: 7767), *DGAT1* (Entrez Gene ID: 8694), *NCOR2* (Entrez
1010 Gene ID: 9612), *IL20* (Entrez Gene ID: 50604), *OTUD4* (Entrez Gene ID: 54726) and *EPB41L5*
1011 (Entrez Gene ID: 57669). The remaining 310 genes were the candidate hits that pass the primary
1012 screens.

1013 In the deconvolution screens, we performed similar analyses for each siRNA
1014 oligonucleotide as that for siRNA pools in the first analysis of the primary screens to assess the
1015 effect of each siRNA oligonucleotide on SIN-induced autophagy and HSV-1 Δ BBD-induced
1016 autophagy. For each candidate gene identified by the primary screens, genes having two or more
1017 oligonucleotides passing the deconvolution screens were considered as the confirmed hits of our
1018 siRNA screens.

1019 ***Bioinformatic analyses of confirmed hits from the deconvolution siRNA screens***

1020 The gene identity (Entrez gene ID) of 216 confirmed siRNA screen hits was first converted to
1021 the Universal Protein Resource (UniProt) protein knowledgebase (UniProtKB) ID using the
1022 Retrieve/ID mapping function (<http://www.uniprot.org>). The gene sets were then analyzed by
1023 DAVID Bioinformatics Resources 6.8 (<https://david.ncifcrf.gov/>) using the default settings,
1024 including molecular function (MF), biological process (BP) and cellular component (CC)
1025 categories from Gene Ontology (GOTERM), InterPro protein sequence analysis & classification
1026 (INTERPRO), the European Bioinformatics Institute (EMBL-EBI) BioCarta Pathway
1027 (BIOCARTA), Kyoto Encyclopedia of Genes and Genomes PATHWAY Database (KEGG),
1028 UniProt protein knowledgebase (UP), Online Mendelian Inheritance in Man (OMIM), The
1029 Protein Information Resource (PIR), Clusters of Orthologous Groups of proteins (COGs), Simple
1030 Modular Architecture Research Tool (SMART) and the Biological Biochemical Image Database
1031 (BBID)^{48,49}. Hypergeometric tests were performed to assess the enrichment of each functional
1032 gene set for the confirmed siRNA hits. The enrichment score was defined as -
1033 \log_{10} (hypergeometric test *P*-value). Enriched gene sets having false discovery rate (FDR)
1034 adjusted *P*-values below 0.05 were considered as terms that were significantly enriched. All
1035 computations were conducted in the R environment version 3.5.1 (www.r-project.org).

1036 To construct a functional enrichment network graph, the above enrichment results were
1037 plotted as a graph with nodes denoting enriched gene sets. The size of each node corresponds to
1038 the number of confirmed siRNA hits and the color intensity, which is scaled according to the
1039 enrichment score. The thickness and color intensity of lines connecting two nodes represent the
1040 extent of overlap between two gene sets, which was calculated using the following formula:

$$1041 \text{Extent of overlap (Set A | Set B)} = \frac{\text{Number of overlapping genes}}{\text{Number of genes in Set A} + \text{Number of genes in Set B} - \text{Number of overlapping genes}}.$$

1042 ***RNA interference in follow-up study of confirmed siRNA screen hits***

1043 RNA interference was performed to knock down the expression of target genes in HeLa cells
1044 cultured in either 10-cm petri dishes or 6-well plates. Cells were reverse transfected with specific
1045 siRNA oligonucleotides using Invitrogen Lipofectamine RNAiMAX according to the
1046 manufacturer's instruction for 72 h. Knockdown efficiency of target genes was confirmed by
1047 either western blot analysis or quantitative real-time PCR analysis.

1048 ***Quantitative real-time PCR (qRT-PCR) analysis***

1049 Total RNA was extracted from HeLa cells using an RNeasy Plus Mini Kit (Qiagen) and further
1050 treated with DNase I (New England Biolabs) to remove residual genomic DNA contamination.
1051 Complementary DNA (cDNA) was synthesized using 1 µg purified RNA, oligo-dT primer and
1052 an iScript cDNA Synthesis Kit (Bio-Rad Laboratories). Relative gene expression levels were
1053 assessed using QuantiFast SYBR Green PCR Kit (Qiagen) on a 7500 Fast Real-Time PCR
1054 System (Applied Biosystems). The qRT-PCR primers for human *SNX32*, *SNX5*, *IFN-β*, *IFIT1*
1055 and *β-actin* (internal control) used in this study are as follows: *SNX32* forward primer, 5'-
1056 TGGCTTCCGATGAGGACCTGAA-3'; *SNX32* backward primer, 5'-
1057 CCTTGTTGGCATTCTCGTAGTCG-3'; *SNX5* forward primer, 5'-
1058 CAGAGCCCAGAGTTTTCTGTTAC-3'; *SNX5* backward primer, 5'-
1059 CCCAGCATAGTCTGTTGTTTCA-3'; *IFN-β* forward primer, 5'-
1060 ATGACCAACAAGTGTCTCCTCC-3'; *IFN-β* backward primer, 5'-
1061 GGAATCCAAGCAAGTTGTAGCTC-3'; *IFIT1* forward primer, 5'-
1062 TTGATGACGATGAAATGCCTGA-3'; *IFIT1* backward primer, 5'-
1063 CAGGTCACCAGACTCCTCAC-3'; *β-actin* forward primer, 5'-CTGGCACCCAGCACAATG-
1064 3'; *β-actin* backward primer, 5'-GCCGATCCACACGGAGTACT-3'.

1065 ***Assessment of viral entry***

1066 To compare viral entry efficiency between cell lines, we used a qRT-PCR-based approach to
1067 assess relative quantity of SIN minus strand RNA and the HSV-1 immediate early gene ICP27
1068 transcript as their levels correlate with genomic contents of incoming virions in the
1069 cytoplasm^{50,51}. HeLa cells were incubated with either SIN (MOI = 50) or HSV-1ΔBBD (MOI =
1070 25) viral inoculum (in Opti-MEM I Reduced Serum Medium) for 1 h on ice in a 4°C cold room,
1071 and then rinsed five times with ice-cold Opti-MEM I Reduced Serum Medium to remove
1072 unbound virions. Cells were either collected immediately (t = 0 h) or further cultured in fresh
1073 warm Opti-MEM I Reduced Serum Medium supplemented with 5% HI FBS for 2 h at 37°C to
1074 allow viral entry, and then collected by digestion with 0.25% trypsin-EDTA for 5 min at 37°C.
1075 RNA extraction and cDNA was performed as described above in the “Quantitative real-time
1076 PCR analysis” section. For HSV-1 infection, relative mRNA levels of viral immediate early gene
1077 *ICP27* were normalized to that of β -*actin* (internal control). For SIN infection, cDNA synthesis
1078 was performed using Invitrogen SuperScript III First-Strand Synthesis System for RT-PCR Kit
1079 (Thermo Fisher Scientific). Two sets of cDNA were made using either Oligo-dT primer or SIN
1080 minus-strand RNA-specific primer (SINmsrp), and then used to assess mRNA levels of β -*actin*
1081 (internal control) and SIN minus-strand RNA, respectively. The relative quantity of SIN minus-
1082 strand RNA was normalized to that of β -*actin* mRNA. Primers used in this assay were as
1083 follows: HSV-1 *ICP27* forward primer, 5'-GCGTCGGTCACGGCATAAGG-3'; HSV-1 *ICP27*
1084 backward primer, 5'-CGATGACTTACTGGCGGGTG-3'; SINmsrp, 5'-
1085 CTAAAGACTTGAAAGTCATAGCTG-3'; SIN forward primer, 5'-
1086 CACCCCGCACAAAATGAC-3'; SIN backward primer, 5'-
1087 AAAAGGGCAAACAGCCAATC-3'.

1088 ***Methods for monitoring autophagy induction***

1089 To monitor autophagy in HeLa cells, we assessed LC3-I to LC3-II conversion and p62/SQSTM1
1090 levels by western blot analyses and performed GFP-LC3, PI3P and WIPI2 fluorescence
1091 microscopy. For viral infection experiments, HeLa cells were mock-infected with Opti-MEM I
1092 Reduced Serum Medium containing 5% HI FBS (normal medium) or infected at 37°C for 1.5 h
1093 with normal media containing certain viruses at an MOI of 20 (for CVB3 and poliovirus), 10 (for
1094 CHIKV, IAV, SIN, WNV and Zika virus), and 5 (for HSV-1ΔBBD), respectively. After removal
1095 of virus-containing media, cells were cultured in fresh normal medium for an additional 3 h for
1096 fluorescence microscopic analyses or 4.5 h for western blot detection of LC3-I/II, p62/SQSTM1,
1097 ATG7, ATG13 and actin. For mTOR inhibition and nutrient-deprivation experiments, HeLa cells
1098 were cultured in normal media containing either 250 nM torin 1 or an equivalent volume of
1099 DMSO, or Earle's Balanced Salt Solution (EBSS, Thermo Fisher Scientific) for 1 h at 37°C. To
1100 monitor autophagic flux, bafilomycin A1 (final concentration 100 nM), a lysosomal inhibitor,
1101 was added to culture media at 1 h prior to fixation (in fluorescence microscopy experiments) or 2
1102 h prior to cell collection (in western blot experiments).

1103 ***Fluorescence microscopy and image analyses***

1104 HeLa cells on Nunc Lab-Tek II 4-well glass chamber slides (Thermo Fisher Scientific) were
1105 quickly rinsed once with cold DPBS containing Ca²⁺ and Mg²⁺ (DPBS-CaMg; Sigma-Aldrich)
1106 and then fixed with 3% PFA in DPBS-CaMg for 10 min at room temperature. After removal of
1107 the fixative, cells were rinsed once with DPBS-CaMg. For GFP-LC3 fluorescence microscopy
1108 using HeLa/GFP-LC3 cells, slides were directly mounted with VECTASHIELD Antifade
1109 Mounting Medium with DAPI (Vector Laboratories H-1200) and stored at 4°C until imaging. For
1110 immunofluorescence microscopy using HeLa cells, cells were permeabilized in 0.2% saponin in
1111 DPBS (Sigma-Aldrich D8537) for 15 min at room temperature and then incubated with blocking

1112 buffer (DPBS containing 1% BSA and 0.1% saponin) for an additional 30 min. HeLa cells were
1113 stained with primary antibodies for 1 h at room temperature and rinsed three times with DPBS.
1114 HeLa cells were then incubated with Alexa Fluor secondary antibodies for 1 h at room
1115 temperature, rinsed five times with DPBS, mounted with VECTASHIELD Antifade Mounting
1116 Medium with DAPI (Vector Laboratories H-1200) or ProLong Diamond Antifade Mountant with
1117 DAPI (Thermo Fisher Scientific P36961) and stored at 4°C until imaging. For PI3P fluorescence
1118 microscopy, HeLa cells were fixed with 4% PFA in DPBS-CaMg for 20 min at room
1119 temperature followed by a single quick wash with DMEM. Cells were permeabilized with DPBS
1120 containing 0.1% N-lauroylsarcosine sodium (Sigma-Aldrich L9150) and 2% BSA for 5 min, and
1121 then incubated with a PI3P-specific fluorescent probe PX-Alexa555^{28,52} for 15 min. After
1122 washing with DPBS containing 2% BSA twice, slides were mounted with ProLong Diamond
1123 Antifade Mountant with DAPI and stored at 4°C until imaging. To minimize fluorescent signal
1124 decay, slides were imaged on the second day after mounting.

1125 Fluorescent micrographs were acquired using a Zeiss Axio Imager Z2 microscope equipped
1126 with a Photometrics CoolSnap HQ2 CCD camera using a Zeiss PLAN APOCHROMAT 20X/0.8
1127 NA wide-field objective or PLAN APOCHROMAT 40X/0.9 NA oil immersion objective. Z-
1128 stack images were acquired with the same acquisition times (for each primary antibody) for
1129 samples prepared in each batch of experiment. Z-stack images were deconvolved with
1130 AutoQuant version X2 (Media Cybernetics) and further analyzed with Imaris version 9.3.0
1131 (Bitplane Inc.) using the same settings for each batch of samples. Background thresholding using
1132 secondary antibody control staining was applied for all experiments. Random images were
1133 chosen from greater than 100 cells per well of triplicate samples for each condition for analysis
1134 by an observer blinded to experimental condition.

1135 ***Acid bypass assay***

1136 To determine whether viral entry at the plasma membrane triggers autophagy, HeLa/GFP-LC3
1137 cells in Nunc Lab-Tek II 4-well glass chamber slides were rinsed once with ice-cold Opti-MEM
1138 I Reduced Serum Medium (Opti-MEM) and incubated in ice-cold Opti-MEM on ice for 10 min
1139 in a 4°C cold room. Cells were then incubated in virus-free ice-cold Opti-MEM (mock infection)
1140 or ice-cold Opti-MEM containing SIN (strain SVIA, MOI = 50) or HSV-1ΔBBD (MOI = 25) on
1141 ice in a 4°C cold room for 1 h to allow viral attachment to cell surface. After discarding viral
1142 inocula, cells were rinsed three times with ice-cold Opti-MEM to remove unbound virions. Cells
1143 were then incubated with ice-cold Opti-MEM (pH 7.4) or acidic Opti-MEM (pH 5.4) for 10 min
1144 at 4°C. The pulse of acidic treatment leads to fusion between the viral envelope and cellular
1145 plasma membrane, and thus viral entry occurs at the plasma membrane instead of conventional
1146 endolysosomal routes (which is therefore called an “acid bypass”). The medium was replaced
1147 with warm fresh Opti-MEM supplemented with 5% HI FBS (normal medium) and cells were
1148 cultured for 2 h at 37°C (to allow viral entry in the control group without acid bypass treatment).
1149 The medium was replaced with warm fresh normal medium and cells were further cultured for
1150 an additional 2.5 h at 37°C. GFP-LC3 fluorescence microscopy was performed as described in
1151 the section “*Fluorescence microscopy and image analyses*”. To compare viral entry efficiency in
1152 HeLa cells receiving the two types of pulse treatments (pH 5.4 versus pH 7.4), viral infection
1153 was performed similarly as described above except that cells were collected at the end of 2-hour
1154 culture at 37°C (without medium change and without an additional 2.5-hour culture). Viral entry
1155 efficiency was then examined similarly as described in the section “*Assessment of viral entry*”.

1156 ***Assessment of bacterial xenophagy***

1157 To study autophagic capture of Group A *Streptococcus* (xenophagy), Group A *Streptococcus*
1158 was grown to mid-log phase and collected by centrifugation at 3,000 g for 5 min. Bacterial
1159 pellets were rinsed three times with Opti-MEM I Reduced Serum Medium (Opti-MEM). The
1160 OD₆₀₀ of bacteria resuspended in Opti-MEM was determined using a GENESYS 30 Visible
1161 Spectrophotometer (Thermo Fisher Scientific) and the number of viable bacteria (colony-
1162 forming unit [cfu]) was determined on Blood Agar (TSA with 5% Sheep Blood) Plates (Thermo
1163 Fisher Scientific). To infect wild-type and *SNX5*^{KO} HeLa/GFP-LC3 cells, cells were incubated
1164 with antibiotic-free Opti-MEM supplemented with 5% FBS containing Group A *Streptococcus*
1165 (at an MOI of 50) for 1 h at 37°C. Cells were washed two times with Opti-MEM to remove
1166 unbound bacteria, and then cultured in fresh Opti-MEM supplemented with 5% FBS and
1167 antibiotics (100 µg/ml gentamicin and 100 U/ml penicillin G, which kill the extracellular
1168 bacteria) for an additional three hours at 37°C. Cells were then fixed for fluorescence
1169 microscopy analysis as described in the section “*Fluorescence microscopy and image analyses*”.

1170 ***Endolysosomal LC3 lipidation induced by osmotic imbalance***

1171 Wild-type and *SNX5*^{KO} HeLa/GFP-LC3 cells were cultured in Opti-MEM I Reduced Serum
1172 Medium supplemented with 5% FBS (normal medium) in Nunc Lab-Tek II 4-well glass chamber
1173 slides overnight. Hypotonic medium was made by mixing fresh normal medium with sterile
1174 water (Sigma-Aldrich W4502) at a ratio of 20:80 (vol/vol). Cells were rinsed three times with
1175 DPBS (Sigma-Aldrich D8537) and then cultured in fresh normal medium or hypotonic medium
1176 for 1 h. Cells were fixed and immunofluorescence microscopy was performed using the protocol
1177 described in the section “*Fluorescence microscopy and image analyses*” and stained for the early
1178 endosomal marker EEA1 and the lysosomal marker LAMP1.

1179 ***Monensin-driven LC3-associated phagocytosis of latex beads***

1180 Wild-type and *SNX5*^{KO} HeLa/GFP-LC3 cells (80,000 cells/well) were cultured in Opti-MEM I
1181 Reduced Serum Medium supplemented with 5% FBS (normal medium) in Nunc Lab-Tek II CC2
1182 4-well glass chamber slides (Thermo Fisher Scientific) overnight. Polybead Microspheres (3.00
1183 μm in diameter) (Polysciences Inc. 17134-15) were washed twice by resuspending the beads in
1184 sterile PBS and pelleting for 5 min at 2,500 g. Cells were incubated with fresh normal medium
1185 containing beads (approximately 50 beads per cells) for 4 h. Cells were rinsed three times with
1186 sterile PBS to remove unengulfed beads and cultured for 45 min in fresh normal medium
1187 containing 100 μM monensin or an equivalent volume of solvent control (ethanol). Cells were
1188 rinsed twice with cold PBS and then fixed in ice-cold methanol for 4 min in -20°C . Cells were
1189 rinsed twice with PBS and blocked in PBS containing 2% BSA (blocking buffer) for 30 min at
1190 room temperature. Cells were incubated with blocking buffer containing goat anti-LAMP1
1191 polyclonal antibody for 1 h at room temperature. Cells were rinsed three times in PBS, and then
1192 incubated with blocking buffer containing Alexa Fluor 594 secondary antibody for 1 h at room
1193 temperature. Cells were rinsed five times with PBS and slides were mounted with ProLong
1194 Diamond Antifade Mountant with DAPI and stored at 4°C until imaging. Intracellular structures
1195 containing latex beads were studied with immunofluorescence microscopy and differential
1196 interference contrast (DIC) microscopy (also known as Nomarski interference contrast
1197 microscopy).

1198 ***Glucose transporter 1 (GLUT1) lysosomal sorting assay***

1199 Retromer activity was monitored by a GLUT1 lysosomal sorting assay as previously described⁵³,
1200 in which lysosomal localization of mis-sorted GLUT1 serves as an indicator of defective
1201 retromer activity. HeLa cells were transfected with NC control siRNAs or siRNAs targeting
1202 *SNX5*, *SNX32*, *VPS29* and *ATG7* for 72 h. Immunofluorescence microscopy was performed

1203 using the protocol described in the section “*Fluorescence microscopy and image analyses*” with
1204 staining for GLUT1 and LAMP1. Quantitative analyses of colocalization between GLUT1 and
1205 LAMP1 (Manders’ overlap coefficient) were performed using the ImarisColoc module of Imaris
1206 version 9.3.0 (Bitplane Inc.).

1207 ***Transferrin receptor recycling assay***

1208 To assess the fast and slow recycling activity of plasma membrane-anchored receptors through
1209 endocytic pathways in HeLa cells, a pulse-chase transferrin receptor recycling assay was
1210 performed as follows. Wild-type and *SNX5*^{KO} HeLa cells (12,000 cells/well) were seeded in 96-
1211 well stripwell plates (Corning) at 80% confluency one day prior to the experiment. Cells were
1212 first rinsed three times with 200 μ L assay buffer PBS⁴⁺ (PBS supplemented with 1 mM CaCl₂, 1
1213 mM MgCl₂, 0.2% BSA and 5 mM D-glucose) and then cultured in 100 μ L PBS⁴⁺ for 30 min at
1214 37°C to minimize the background biotin signal. Cells were chilled down in 100 μ L ice-cold
1215 PBS⁴⁺ on ice in a 4°C cold room for 5 min, and then incubated with 100 μ L PBS⁴⁺ (blank
1216 controls) or PBS⁴⁺ containing 5 μ g/mL Biotin-transferrin (Biotin-Tfn) (Sigma-Aldrich T3915).
1217 The blank controls were left on ice until fixation. Biotin-Tfn-treated cells were cultured at 37°C
1218 for either 10 min or 30 min to allow uptake of Biotin-Tfn into cells, which corresponds to the
1219 assessment of fast recycling pathway or slow recycling pathway, respectively. Biotin-Tfn uptake
1220 was stopped by replacing the buffer with 200 μ L fresh ice-cold PBS⁴⁺ and cells were rapidly
1221 cooled on ice. Cells were rinsed once with ice-cold PBS⁴⁺ to remove excess of unbound Biotin-
1222 Tfn in wells. Cells were then treated with avidin and biocytin to mask surface bound Biotin-Tfn
1223 as follows. First, cells were incubated in 50 μ L ice-cold PBS⁴⁺ containing 50 μ g/mL Invitrogen
1224 avidin (Thermo Fisher Scientific 434401) on ice for 10 min. Cells were rinsed twice with ice-
1225 cold PBS⁴⁺, and then incubated in 50 μ L ice-cold PBS⁴⁺ containing 5 μ g/mL Invitrogen biocytin

1226 (Thermo Fisher Scientific B1592) on ice for 15 min to mask cell surface-bound Biotin-Tfn. Cells
1227 were rinsed twice with ice-cold PBS⁴⁺, and one strip of cells was temporarily stored on ice until
1228 fixation, which served as the “initial total intracellular Biotin-Tfn content” controls (i.e. t = 0
1229 min) for the following chase steps. The remaining strips of cells were cultured in 100 μL PBS⁴⁺
1230 containing 2 mg/mL (saturation concentration) holo-transferrin (Sigma-Aldrich T4132) at 37°C
1231 for serial chase times (2.5, 5, 10, 20 and 30 min) to allow recycling of endosomal biotin-Tfn-
1232 bound Tfn receptor to the cell surface. To stop the recycling, the buffer was replaced with 100
1233 μL fresh ice-cold PBS⁴⁺. Cells were further rapidly rinsed three times with 200 μL ice-cold wash
1234 buffer (200 mM acetic acid, 200 mM NaCl, pH 2.3) for 15 sec each wash to remove plasma
1235 membrane-associated Biotin-Tfn. All strips of cells were rinsed three times with 200 μL ice-cold
1236 PBS, and fixed in 100 μL 4% PFA in PBS for 30 min at 37°C. Cells were rinsed three times with
1237 200 μL ice-cold PBS, and permeabilized in PBS containing 0.1% Triton X-100 for 5 min at
1238 room temperature. Cells were blocked with casein blocking buffer (Sigma-Aldrich B6429) for an
1239 additional 30 min at room temperature. Cells were incubated with 200 μL Q-PBS buffer (pH 7.4)
1240 containing 2% BSA, 0.1% lysine, 0.01% saponin and streptavidin-HRP (Roche; 1:10,000) for 1
1241 h. Cells were rinsed six times with 200 μL PBS for 5 min each wash, and incubated with 200 μL
1242 o-phenylenediamine dihydrochloride (OPD) solution (Sigma-Aldrich) for 20 min. Reactions
1243 were stopped by adding 50 μL 5M H₂SO₄ solution. Absorbance at 490 nm and 650 nm was
1244 determined using a Synergy H1 Hybrid Multi-Mode Reader (BioTek Instruments). To determine
1245 the total protein levels in each well, cells were rinsed five times with 200 μL PBS, and then
1246 incubated with 100 μL Pierce BCA Solution (Thermo Fisher Scientific) on a shaker for 30 min at
1247 60°C. Absorbance at 562 nm was determined using a Synergy H1 Hybrid Multi-Mode Reader
1248 (BioTek Instruments). HRP activity was normalized to protein concentration for each well. The

1249 percentage of remaining intracellular Biotin-Tfn content for each chase time point was calculated
1250 in reference to the initial total intracellular Biotin-Tfn content.

1251 ***Epidermal growth factor receptor (EGFR) endolysosomal degradation assay***

1252 Endolysosomal function of HeLa cells was assessed by an epidermal growth factor (EGF)-
1253 induced EGFR endolysosomal degradation assay. HeLa cells (180,000 cells/well in 6-well
1254 plates) were cultured overnight in DMEM supplemented with 10% FBS, 100 units/mL penicillin
1255 and 100 µg/mL streptomycin. Cells were then starved for 16 h in serum-free DMEM and treated
1256 with DMEM containing 30 µg/mL cycloheximide for 30 min to suppress protein synthesis. Cells
1257 were stimulated with 100 ng/mL EGF (Thermo Fisher Scientific PHG0313), and collected at 0,
1258 0.5, 1, 2 and 4 h, respectively. EGFR and actin protein levels were analyzed by western blot
1259 analysis. Western blot images were collected using a G:Box Chemi Gel Doc System (Syngene)
1260 and densitometry analysis of protein bands was performed using the software GeneTools version
1261 4.3.10.0 (Syngene). Relative EGFR protein levels were normalized to corresponding actin
1262 controls and then converted to percentage values in reference to unstimulated cells (t = 0 h).

1263 ***Viral infectivity assays and viral growth curves***

1264 Viral infection in cultured cells was examined by viral infectivity assays, multi-step growth
1265 curves and single-step growth curves. For the viral infectivity assay, HeLa cells were seeded in
1266 12-well plates (100,000 cells per well) in Opti-MEM I Reduced Serum Medium supplemented
1267 with 5% HI FBS (normal medium) one day prior to infection. Confluent cell monolayers were
1268 incubated with 2-fold serially diluted viral inoculum in normal medium for 1.5 h. After removal
1269 of viral inocula, cells were cultured in 1× MEM supplemented with 1% HI FBS and 1%
1270 methylcellulose (Sigma-Aldrich M0512) for 3 days. Cell monolayers were fixed in methanol for
1271 15 min at room temperature and then stained in 1× crystal violet solution (containing 0.5%

1272 crystal violet and 25% methanol). The numbers of plaques on cell monolayers correspond to the
1273 numbers of cells that established infection during primary infection with viral inoculum, as
1274 methylcellulose blocks viral spread through culture medium without affecting viral direct cell-to-
1275 cell transmission. Thus, plaque numbers normalized to viral input for each well indicate the
1276 relative magnitude of cellular susceptibility to viral infection (i.e. viral infectivity) for each cell
1277 line.

1278 To assess viral multi-step growth and single-step growth in HeLa cells, cell monolayers were
1279 infected with viral inoculum in Opti-MEM I Reduced Serum Medium supplemented with 5% HI
1280 FBS (normal medium) at MOI of 0.01 and 10 for 1.5 h, respectively. After removal of viral
1281 inocula, cells were cultured in fresh normal medium for up to 6 days. Viral multi-step growth in
1282 primary MEFs were assessed similarly as described above, except that MEFs were cultured using
1283 DMEM supplemented with 10% HI FBS. Viral titers at selected time points were determined by
1284 plaque assay.

1285 ***Co-immunoprecipitation (co-IP)***

1286 To investigate the interaction between endogenous proteins, HeLa cells were treated with PIK-III
1287 (5 μ M) or DMSO for 1 h. HeLa cells were lysed in ice-cold 1 \times lysis buffer (pH 7.5) containing
1288 50 mM HEPES, 150 mM NaCl, 1 mM EDTA, 10% glycerol, 1% Triton X-100, cComplete
1289 proteinase inhibitor cocktail (Roche) and Halt phosphatase inhibitor cocktail (Thermo Fisher
1290 Scientific) on ice for 30 min, and further homogenized by passage through 18-gauge needles
1291 fitted onto sterile plastic syringes fifteen times. The insoluble fraction of cell lysates was
1292 removed by centrifugation at 10,000 g and 4 $^{\circ}$ C for 15 min. Cell lysates were further cleared by
1293 incubation with 10 μ L Protein G PLUS-agarose beads (Santa Cruz Biotechnology) for 30 min at
1294 4 $^{\circ}$ C followed by centrifugation at 1,000 g and 4 $^{\circ}$ C for 1 min. The total protein concentration of

1295 supernatants was determined using a Quick Start Bradford Protein Assay Kit (Bio-Rad
1296 Laboratories), and adjusted to the same concentration by adding 1× lysis buffer. Cell lysates
1297 (equivalent volume for each experimental group) were incubated with anti-beclin 1 and anti-
1298 SNX5 antibodies or an appropriate control IgG for 3 h at room temperature, and then subjected
1299 to immunoprecipitation by the addition of 25 µL Protein G PLUS-Agarose beads (Santa Cruz
1300 Biotechnology) for 1 h at room temperature. Agarose beads were pelleted by centrifugation at
1301 1,000 g and 4°C for 1 min and washed five times with ice-cold 1× lysis buffer.
1302 Immunoprecipitates were eluted by boiling agarose beads in 2× Laemmli sample buffer (Bio-Rad
1303 Laboratories) containing 5% β-mercaptoethanol (Bio-Rad Laboratories) for 5 min and then
1304 analyzed by western blot.

1305 ***Western blot analyses***

1306 HeLa cell lysates were prepared by incubating cells with ice-cold 1× lysis buffer (pH 7.5)
1307 containing 50 mM HEPES, 150 mM NaCl, 1 mM EDTA, 10% glycerol, 1% Triton X-100,
1308 cOmplete proteinase inhibitor cocktail (Roche) and Halt phosphatase inhibitor cocktail (Thermo
1309 Fisher Scientific) on ice for 30 min. Cell lysates were then centrifuged at 10,000 g and 4°C for 15
1310 min to remove the insoluble fraction. The supernatant was then mixed with an equal volume of
1311 2× Laemmli sample buffer (Bio-Rad Laboratories) containing 5% β-mercaptoethanol (Bio-Rad
1312 Laboratories) and boiled for 5 min. Denatured proteins were separated by SDS-PAGE using 4-
1313 20% Mini-PROTEAN TGX precast protein gels (Bio-Rad Laboratories) and transferred to
1314 Immun-Blot PVDF membranes (Bio-Rad Laboratories). Membranes were blocked with blotting-
1315 grade blocker (Bio-Rad Laboratories) or 2% BSA in 1× PBS buffer containing 0.05% Tween 20
1316 (PBST), incubated with primary and secondary antibodies diluted according to manufacturers'
1317 instructions, and washed five times with 1× PBST. Protein bands were visualized with

1318 SuperSignal West Pico PLUS Chemiluminescent Substrate (Thermo Fisher Scientific) on a
1319 BioSpectrum imaging system (Ultra-Violet Products) or Light Labs Ultra Blue X-ray film (Light
1320 Labs). Densitometry analysis of protein bands was performed using the software Multi Gauge
1321 3.0 (FUJIFILM). Relative protein levels were normalized to according actin controls. To further
1322 validate that viral infection induces degradation of p62/SQSTM1 instead of its translocation into
1323 the Trion X-100-insoluble fraction, HeLa cells were also lysed in RIPA buffer (Cell Signaling
1324 Technology) containing 1% SDS after mock or viral infection. Western blot and densitometry
1325 analyses were performed similarly as described above.

1326 ***Expression and purification of Class III phosphatidylinositol 3-kinase (PI3KC3) complexes***

1327 PI3KC3 complexes were prepared using a mammalian expression system from a suspension
1328 culture of HEK293F cells. Expression plasmids for PI3KC3 complex components include
1329 pCAG-OSF-ATG14 for Strep-Flag tagged human ATG14, pCAG-OSF-UVRAG for Strep-Flag
1330 tagged human UVRAG, pCAG-NT-P150 for human VPS15 (also known as p150), pCAG-NT-
1331 VPS34 for VPS34 (also known as PI3KC3 or PIK3C3), and pCAG-NT-beclin1 for beclin 1⁵⁴. To
1332 obtain PI3KC3-C1 complexes (containing ATG14, VPS15, VPS34 and beclin 1) and PI3KC3-
1333 C2 complexes (containing UVRAG, VPS15, VPS34 and beclin 1), two plasmid cocktails (0.5
1334 mg per plasmid per 1 L culture medium), were respectively transfected into HEK293F cells
1335 (when cell density reached 1,000,000 cells/mL) using polyethylenimine (PEI) at the mass ratio
1336 1.5:1 (PEI:plasmids). HEK293F cells were cultured in a 37°C incubator with a humidified
1337 atmosphere with 8% CO₂ in air on an orbital shaker rotating at 120 rpm for three days.

1338 For purification of PI3KC3 complexes, HEK293F cells were collected at 72 h after
1339 transfection by centrifugation at 400 g and 4°C for 20 min. Cell pellets were then lysed in ice-
1340 cold 1× lysis buffer containing 20 mM Tris-HCl (pH 8.0), 150 mM NaCl, 1 mM dithiothreitol

1341 (DTT), 1% Triton X-100 and protease inhibitor cocktail (Roche) on ice for 10 min. After
1342 centrifugation at 13,000 g and 4°C for 30 min, the supernatant was filtrated through a 0.45-µm
1343 filter (Roche). Precleared supernatant was incubated with StrepTactin Sepharose High
1344 Performance resin (GE Healthcare) for 1 h at 4°C. The resin was carefully washed three times
1345 with ice-cold washing buffer containing 100 mM Tris-HCl (pH 8.0), 300 mM NaCl and 1 mM
1346 DTT. PI3KC3 complexes were eluted with 10 mM desthiobiotin (Sigma-Aldrich) and
1347 concentrated by centrifugation using Amicon Ultra-15 Centrifugal Filter Units 100K (EMD
1348 Millipore) at 4°C. Concentrated eluate was further purified by gel filtration using Superose 6
1349 Increase 3.2/300 pre-packed high performance glass columns (GE Healthcare) at 4°C, which were
1350 equilibrated with the gel filtration buffer containing 20 mM Tris-HCl (pH 8.0), 150 mM NaCl
1351 and 1 mM DTT. PI3KC3 complex peak fractions were combined and stored in small aliquots at -
1352 80°C after being snap-frozen in liquid nitrogen. The concentration of PI3KC3 complex eluates
1353 was quantitated using the protein A280 method. The purity of protein complexes was examined
1354 by SDS-PAGE and Coomassie blue staining using GelCode Blue Safe Protein Stain (Thermo
1355 Fisher Scientific 24594) according to the manufacturer's instruction.

1356 ***Amino Acid Sequence Alignment and Secondary Structure Prediction of SNX5 and Closely-***
1357 ***related Sorting Nexins***

1358 Amino acid sequence of nine vertebrate SNX5 homologs and four closely-related human sorting
1359 nexins (SNX1, SNX2, SNX6 and SNX32) were acquired form National Center for
1360 Biotechnology Information (NCBI) Reference Sequences (RefSeq) database. Their NCBI
1361 accession IDs are as follows: zebrafish snx5, NP_999934; frog snx5, NP_001016081; snake
1362 SNX5, XP_025024423; Lizard snx5, XP_003219930; chick SNX5, NP_001006178; mouse
1363 Snx5, NP_001186117; pig SNX5, XP_020933988; chimpanzee SNX5, XP_016792968; human

1364 SNX5, NP_689413; human SNX1, NP_003090; human SNX2, NP_003091; human SNX6,
1365 NP_689419; human SNX32, NP_689973. Amino acid sequence alignment of proteins was
1366 performed using Cluster Omega (<https://www.ebi.ac.uk/Tools/msa/clustalo/>). Protein secondary
1367 structure prediction was performed using the University College London (UCL) PSIPRED
1368 Protein Sequence Analysis Workbench (<http://bioinf.cs.ucl.ac.uk/psipred/>).

1369 ***Expression and purification of recombinant SNX5 proteins***

1370 Wild-type SNX5 and a mutant SNX5 EEE (that carries triple mutations K328E/R330E/K332E)
1371 were prepared using a bacterial expression system. The coding region of SNX5 and SNX5 EEE
1372 were cloned into BamHI/SalI sites of the ppSUMO vector, a modified pET-28a vector that
1373 contains an N-terminal hexa-histidine-tag followed by a SUMO-tag and a recognition site for
1374 SUMO protease, Ulp. The empty vector and SNX5 plasmids were transformed into the
1375 chemically competent *E. coli* strain BL21(DE3) and grown to an optical density at a wavelength
1376 of 600 nm (OD₆₀₀) of 0.8 in 2× YT medium. Protein expression was induced by addition of
1377 0.2 mM isopropyl-β-D-thiogalactopyranoside (IPTG) followed by overnight culture at 16°C.
1378 Cells were lysed in 1× bacterial lysis buffer containing 20 mM Tris (pH 8.0), 500 mM NaCl, and
1379 2 mM β-mercaptoethanol by French pressing using Emulsiflex-C5 (AVESTIN). Cell lysates
1380 were cleared by centrifugation at 15,000 g and 4°C for 1 h. Proteins in the lysates were purified
1381 using 1 mL HisTrap columns (GE Healthcare) and size exclusion chromatography using
1382 Superdex 200 increase 10/300 gel filtration columns (GE Healthcare) equilibrated with a buffer
1383 containing 20 mM Tris (pH 8.0), 150 mM NaCl, and 2 mM DTT. SUMO control, SUMO-SNX5
1384 and SUMO-SNX5 EEE were further concentrated by centrifugation using Amicon Ultra-15
1385 Centrifugal Filter Units 10K (EMD Millipore) and stored in small aliquots at -80°C after being
1386 snap-frozen in liquid nitrogen. Protein concentration and quality was assessed as described

1387 above. Approximately 0.1 nanomole of SUMO control, SUMO-SNX5 and SUMO-SNX5 EEE
1388 was loaded per lane on an SDS-PAGE gel.

1389 ***In vitro binding assay***

1390 To determine whether SNX5 directly binds PI3KC3-C1 or PI3KC3-C2 complexes, 0.2 nanomole
1391 of bacterially-purified SUMO control, SUMO-SNX5 and SUMO-SNX5 EEE were incubated
1392 with PI3KC3-C1 or PI3KC3-C2 complexes on Strep-Tactin resin or empty resin in 1× binding
1393 buffer containing 20 mM Tris-HCl (pH 8.0), 150 mM NaCl, 1 mM DTT, 1% Triton X-100 and
1394 protease inhibitor cocktail (Roche) for 3 h at room temperature. Strep-Tactin resin was pelleted
1395 by centrifugation at 1,000 g for 1 min and washed six times with ice-cold 1× binding buffer.
1396 Captured protein complexes were eluted by boiling resin in 2× Laemmli sample buffer (Bio-Rad
1397 Laboratories) containing 5% β-mercaptoethanol (Bio-Rad Laboratories) for 5 min and then
1398 analyzed by western blot.

1399 ***Liposome preparation***

1400 The lipid substrate for the *in vitro* lipid kinase assay was phosphatidylinositol (PI) incorporated
1401 on Large Unilamellar Vesicles prepared by Extrusion Technique (LUVETs)^{29,30} using a lipid
1402 mixture that resembles endosomal lipid composition^{31,32}. PI-containing liposomes were
1403 composed of 47.5% porcine brain phosphatidylcholine (PC, Avanti Polar Lipids 840053), 23%
1404 porcine brain phosphatidylethanolamine (PE, Avanti Polar Lipids 840022), 10% bovine liver PI
1405 (Avanti Polar Lipids 840042), 9% porcine brain sphingomyelin (SM, Avanti Polar Lipids
1406 860062), 8.5% porcine brain phosphatidylserine (PS, Avanti Polar Lipids 840032), and 2%
1407 protonated phosphatidylinositol 4,5-bisphosphate (PI[4,5]P₂, Avanti Polar Lipids 840046). PI-
1408 free control liposomes were composed of similar lipid composition except that PI was replaced
1409 with PS. Six mM of lipid components were mixed together in 1:1 (vol/vol) chloroform:methanol

1410 and dried in glass tubes under a stream of nitrogen. The lipid film was further vacuum-dried for 2
1411 h at room temperature and then rehydrated into 1× liposome buffer containing 20 mM Tris-HCl
1412 (pH7.5), 150 mM NaCl and 1 mM DTT. Lipids were subjected to ten cycles of freeze and thaw
1413 between liquid nitrogen and a 42°C water bath, and then extruded twenty-one times through
1414 polycarbonate filters with pore sizes of 100 nm or 30 nm in diameter (Avanti Polar Lipids).
1415 These LUVETs of two sizes are respectively designated as “larger” and “smaller” liposomes in
1416 this study. Liposomes were stored in glass vials at 4°C and used for *in vitro* lipid kinase assay
1417 within 24 h.

1418 ***In vitro* lipid kinase assays**

1419 The kinase reactions were performed in 8-tube strip PCR tubes at a ratio of 1:1:1 (vol/vol/vol)
1420 for PI-containing or PI-free liposomes (2 mM of total lipids) (1/3 volume), purified PI3KC3-C1
1421 and varying concentrations of SNX5 diluted in 1× liposome buffer (1/3 volume) and a kinase
1422 reaction buffer containing ATP (1/3 volume; added at the last step to initiate the reaction). The
1423 kinase reaction buffer consisted of 20 mM Tris-HCl (pH7.5), 105 mM NaCl, 30 mM MgCl₂, 1
1424 mM DTT and 300 μM ATP, which has the same osmotic pressure as the 1× liposome buffer. The
1425 reactions were carried out for 30 min at 37°C. ATP consumption in each reaction was assessed
1426 using an ADP-Glo Kinase Assay Kit (Promega).

1427 **Cryogenic electron microscopy (cryo-EM) and assessment of liposomal curvature**

1428 To investigate SNX5-induced liposomal deformation, the “larger” LUVETs (extrusion filter pore
1429 size: 100 nm in diameter) containing 2 mM total lipids were incubated with 800 nM of SUMO
1430 control, SUMO-SNX5 and SUMO-SNX5 EEE in 1× liposome buffer (without PI3KC3-C1 and
1431 ATP) for 30 min at 37°C. Lacey Carbon film 300 mesh Copper grids (Agar Scientific AGS166-
1432 3) were glow-discharged at 30 mA for 40 seconds in a Pelco easiGlow Glow Discharge Cleaning

1433 System (Ted Pella). A drop (3.5 μL) of the suspension was then applied onto the carbon-coated
1434 side of a specimen grid held by forceps in the blotting position inside the environmental chamber
1435 (humidity 100%) of FEI Vitrobot (Thermo Fisher Scientific) at room temperature. Grids were
1436 immediately blotted at a force of 12 for 4 seconds, plunged into the liquid ethane, and then stored
1437 in liquid nitrogen until imaging. The specimens were examined in liquid nitrogen using an FEI
1438 Talos Arctica TEM (Thermo Fisher Scientific). Micrographs were collected at a magnification of
1439 28,000 under 300 kV and low-dose condition (approximately $20 \text{ e}^-/\text{\AA}^2$) using an FEI Eagle 4k \times
1440 4k CCD.

1441 In cryo-EM micrographs, liposomes display in the form of either circular or elliptical shapes
1442 (in two-dimensional space), which correlate with spherical and ellipsoid shapes of the liposome
1443 (in three-dimensional space). For each experimental group, the lengths of the major axis (2a) and
1444 minor axis (2b) of an ellipse were quantitated for at least 150 liposomes per condition. Since the
1445 circle can be considered as a unique ellipse with two foci at the same spot (the center), 2a is
1446 equal to 2b for a circle. Unlike a constant curvature along the circle, an ellipse has continuously
1447 altering curvature with the highest curvature seen at two vertex points. In differential geometry,
1448 the radius of curvature (R), which is the reciprocal of the curvature (κ), inversely correlates with
1449 the magnitude of curvature. The radius of curvature at vertex points of an ellipse was quantitated
1450 and compared between experimental groups.

1451 ***Animal studies***

1452 Animal studies were performed in a barrier facility at the University of Texas Southwestern
1453 Medical Center. Mice were raised under the following housing conditions: ambient temperature,
1454 70°F to 75°F; humidity, 30% to 50%; normal light-dark cycle (lights on 6 a.m. and lights off 6
1455 p.m.); chow, Teklad Global 16% Protein Rodent Diet (Envigo 2916); water, reverse osmosis

1456 water. For *in vivo* studies, intracerebral (i.c.) infection was performed for HSV-1, SIN and WNV,
1457 and subcutaneous infection was performed for CHIKV. All intracerebral infections were
1458 performed by injecting virus diluted in 30 μ L Hank's Balanced Salt Solution (HBSS, Thermo
1459 Fisher Scientific) in the right cerebral hemisphere. For HSV-1 infection, eight- to ten-week-old
1460 littermate $Snx5^{+/+}$ and $Snx5^{-/-}$ mice were infected i.c. with 50,000 plaque-forming units (pfu) of
1461 HSV-1 Δ BBD or HSV-1 Δ BBD-MR. Since HSV-1 Δ BBD-MR is significantly more virulent than
1462 HSV-1 Δ BBD, this strain was also administrated using a lower dose (500 pfu, i.c.) to ensure that
1463 differences observed between $Snx5^{+/+}$ and $Snx5^{-/-}$ mice in susceptibility to infection with HSV-
1464 1 Δ BBD is truly specific for HSV-1 strains that lack the ability to inhibit host autophagy. For SIN
1465 infection, seven-day-old $Snx5^{+/+}$ and $Snx5^{-/-}$ neonatal mice were infected i.c. with 1,000 pfu of
1466 SIN strains dsTE12Q or dsTE12Q.dnAtg5 (SIN.dnAtg5). For WNV infection, 5.5-day-old
1467 $Snx5^{+/+}$ and $Snx5^{-/-}$ neonatal mice were infected i.c. with 1 pfu of WNV strain Egypt-101. For
1468 infection with CHIKV, seven-day-old $Snx5^{+/+}$ and $Snx5^{-/-}$ neonatal mice were infected
1469 subcutaneously with 100,000 pfu of CHIKV strain 06-021 in 30 μ L HBSS. All mice were
1470 monitored daily. Infected animals were randomly chosen for tissue collection at designated time
1471 points post infection. To assess viral loads in mouse brains, 10% (weight/volume) homogenates
1472 of the right hemispheres were prepared by grinding brains in HBSS followed by either three
1473 freeze-thaw cycles (for HSV-1) or no freeze-thaw cycle (SIN), and then assessed by plaque assay
1474 titration. For histopathology studies, the left hemispheres were fixed in 4% PFA, embedded in
1475 paraffin, and further analyzed by immunohistochemistry assays as described below. For
1476 mortality studies, mice that survived from viral infection were euthanized on day 21 post
1477 infection. Since the *in vivo* virulence of SIN.dnAtg5 is much lower than the parental strain
1478 dsTE12Q, SIN.dnAtg5-infected mice were monitored until day 28 post infection and all

1479 surviving mice were euthanized at the end of the experiment. All animal procedures were
1480 performed in accordance with institutional guidelines and with approval from the Institutional
1481 Animal Care and Use Committee of the University of Texas Southwestern Medical Center.

1482 ***Histology***

1483 Five- μ m-thick sagittal sections of mouse brain were prepared using PFA-fixed and paraffin-
1484 embedded samples. Terminal deoxynucleotidyl transferase dUTP nick end labeling (TUNEL)
1485 staining of mouse brain sections was performed using Apoptag Peroxidase In Situ Apoptosis
1486 Detection Kit (EMD Millipore) and SIGMAFAST 3,3'-diaminobenzidine tablets (DAB; Sigma-
1487 Aldrich) according to the manufacturers' instructions. High-resolution montages of the entire
1488 sagittally sectioned mouse brain slides were acquired using a Zeiss Axio Scan.Z1 slide scanner
1489 equipped with a Zeiss PLAN APOCHROMAT 20X/0.8 NA objective (Carl Zeiss Microscopy),
1490 and then analyzed with NDP.view version 2.3.13 (Hamamatsu Photonics). The number of
1491 TUNEL-positive foci per mouse brain sections was determined by an observer blinded to
1492 experimental condition.

1493 ***Statistical analyses***

1494 Statistical analyses for genome-wide siRNA screens are described in the section "*High-content*
1495 *image-based genome-wide siRNA screens*". Where appropriate, two-sided statistical tests were
1496 used throughout this study. For Kaplan-Meier survival curves in animal studies, log-rank tests
1497 (two-sided) were performed using the software Prism 8 version 8.3.0 (GraphPad Software). For
1498 *in vivo* pathogenesis analysis and all the *in vitro* assays, *P* values were determined using the
1499 open-source R software package version 3.6.2 (www.r-project.org). Unpaired two-tailed *t*-tests
1500 were used for comparisons of two means, and one-way ANOVA analysis with Dunnett's test for
1501 multiple comparisons was performed to assess the significance of multiple experimental groups

1502 versus a control condition. Two-way ANOVA analysis was performed to assess the significance
1503 of the interaction of two independent variables. Linear regression analysis was used to assess the
1504 dose-dependent effect of a variable, and two- or three-way interaction terms in these linear
1505 models were then used to determine the significance of differences of dose-dependent effects
1506 between different treatment groups.

1507

1508 **Data availability**

1509 All relevant data supporting the findings of this study are available within the manuscript and its
1510 supplementary information files. All figures, including Figs. 1 - 3 and Extended Data Figs. 1, 3 -
1511 10 have associated raw data. Original blots are available in Supplementary Fig. 1. Original
1512 protein sequences were acquired from the NCBI RefSeq database, and the link to this database
1513 and protein accession numbers are provided in the Amino Acid Sequence Alignment section of
1514 the Methods.

1515

1516 **Code availability**

1517 Custom codes (for R packages) used in siRNA screen analyses are available from the GitHub
1518 database (<https://github.com/xiao-zang/snx5>).

1519

1520 **Additional References**

- 1521 38. van Weering, J. R. *et al.* Molecular basis for SNX-BAR-mediated assembly of distinct
1522 endosomal sorting tubules. *EMBO J* **31**, 4466-4480 (2012).
- 1523 39. Durkin, M. E., Qian, X., Popescu, N. C. & Lowy, D. R. Isolation of mouse embryo
1524 fibroblasts. *Bio Protoc* **3**, e908 (2013).

- 1525 40. Dowdle, W. E. *et al.* Selective VPS34 inhibitor blocks autophagy and uncovers a role for
1526 NCOA4 in ferritin degradation and iron homeostasis in vivo. *Nat Cell Biol* **16**, 1069-1079
1527 (2014).
- 1528 41. Thoreen, C. C. *et al.* An ATP-competitive mammalian target of rapamycin inhibitor
1529 reveals rapamycin-resistant functions of mTORC1. *J Biol Chem* **284**, 8023-8032 (2009).
- 1530 42. Gobeil, P. A. & Leib, D. A. Herpes simplex virus gamma34.5 interferes with
1531 autophagosome maturation and antigen presentation in dendritic cells. *MBio* **3**, e00267-
1532 00212 (2012).
- 1533 43. Taylor, R. M., Hurlbut, H. S., Work, T. H., Kingston, J. R. & Frothingham, T. E. Sindbis
1534 virus: a newly recognized arthropodtransmitted virus. *Am J Trop Med Hyg* **4**, 844-862
1535 (1955).
- 1536 44. Hardwick, J. M. & Levine, B. Sindbis virus vector system for functional analysis of
1537 apoptosis regulators. *Methods Enzymol* **322**, 492-508 (2000).
- 1538 45. Schuffenecker, I. *et al.* Genome microevolution of chikungunya viruses causing the
1539 Indian Ocean outbreak. *PLoS Med* **3**, e263 (2006).
- 1540 46. Keller, B. C. *et al.* Resistance to alpha/beta interferon is a determinant of West Nile virus
1541 replication fitness and virulence. *J Virol* **80**, 9424-9434 (2006).
- 1542 47. Melnick, J. L. *et al.* Isolation from human sera in Egypt of a virus apparently identical to
1543 West Nile virus. *Proc Soc Exp Biol Med* **77**, 661-665 (1951).
- 1544 48. Huang da, W., Sherman, B. T. & Lempicki, R. A. Systematic and integrative analysis of
1545 large gene lists using DAVID bioinformatics resources. *Nat Protoc* **4**, 44-57 (2009).

- 1546 49. Huang da, W., Sherman, B. T. & Lempicki, R. A. Bioinformatics enrichment tools: paths
1547 toward the comprehensive functional analysis of large gene lists. *Nucleic Acids Res* **37**, 1-
1548 13 (2009).
- 1549 50. Honess, R. W. & Roizman, B. Regulation of herpesvirus macromolecular synthesis. I.
1550 Cascade regulation of the synthesis of three groups of viral proteins. *J Virol* **14**, 8-19
1551 (1974).
- 1552 51. Sawicki, D. L., Sawicki, S. G., Keranen, S. & Kaariainen, L. Specific Sindbis virus-
1553 coded function for minus-strand RNA synthesis. *J Virol* **39**, 348-358 (1981).
- 1554 52. Axe, E. L. *et al.* Autophagosome formation from membrane compartments enriched in
1555 phosphatidylinositol 3-phosphate and dynamically connected to the endoplasmic
1556 reticulum. *J Cell Biol* **182**, 685-701 (2008).
- 1557 53. Steinberg, F. *et al.* A global analysis of SNX27-retromer assembly and cargo specificity
1558 reveals a function in glucose and metal ion transport. *Nat Cell Biol* **15**, 461-471 (2013).
- 1559 54. Ma, M. *et al.* Cryo-EM structure and biochemical analysis reveal the basis of the
1560 functional difference between human PI3KC3-C1 and -C2. *Cell Res* **27**, 989-1001 (2017).

1 **Supplementary Table 1.**

2 Statistical analysis for primary siRNA screens using a mixed-effects Poisson regression model in
3 which GFP-LC3 puncta numbers/cell served as response variable, siRNA treatment (using
4 negative control wells as references) served as the independent variable, and a random intercept
5 was included to model the correlated observations among cells within each well.

6

7 **Supplementary Table 2.**

8 Statistical analysis of primary siRNA screens using a mixed-effects Poisson regression model in
9 which GFP-LC3 puncta numbers/cell served as response variable, random intercepts were used
10 to account for correlated intra- and inter-cell observations in the same assay plate, and fixed
11 effects included siRNA treatment and viral infections with their interactions.

12

13 **Supplementary Table 3.**

14 Statistical analysis results for deconvolution siRNA screens. Shown are the scores (coefficient
15 values) and Wald-test *P*-values (two-sided) for each Dharmacon siRNA oligonucleotide
16 corresponding to 310 genes that scored positive in the primary siRNA screens and for each assay
17 plate. “N/A”, failed regression of statistical models. NC, non-targeting control siRNA.

18

19 **Supplementary Table 4.**

20 Data from Extended Data Fig. 2g with additional details including Entrez gene ID, UniProtKB
21 ID, gene name, subcellular location, function, and gene involvement in all the categories from
22 several gene ontology databases (such as GO Terms, INTERPRO, UP, SMART, PIR, KEGG,
23 BIOCARTA, COG, BBID and OMIM).

24

25 **Supplementary Table 5.**

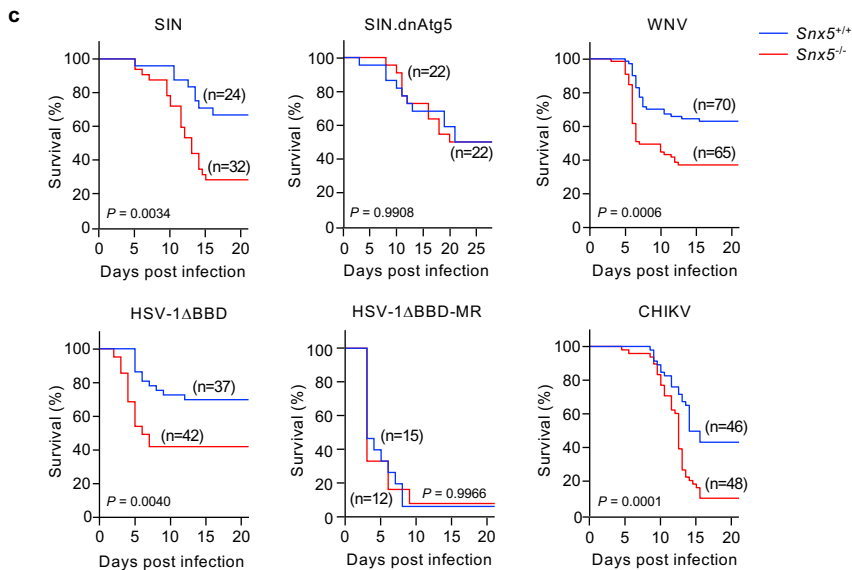
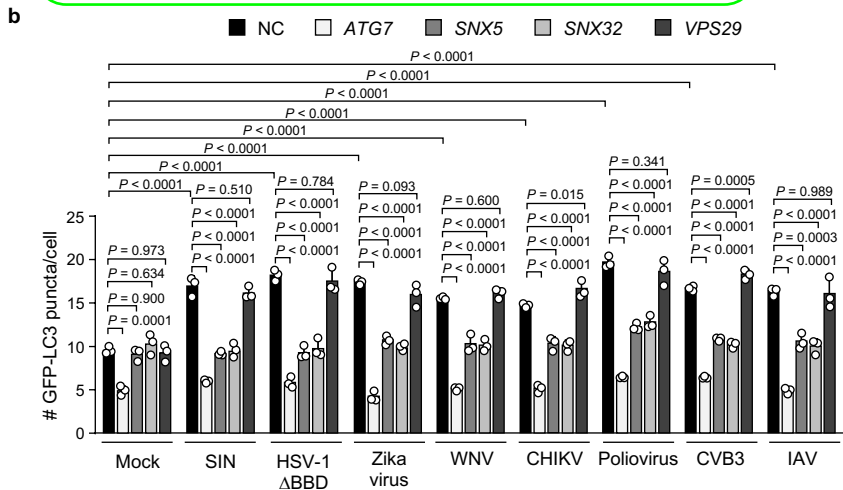
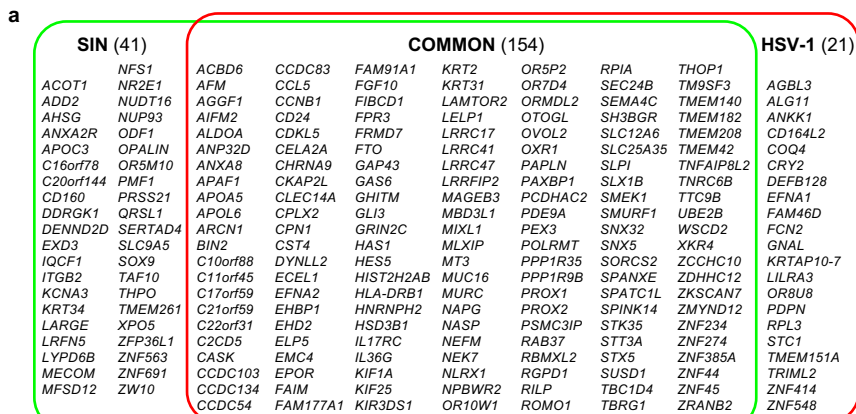
26 Data from Extended Data Fig. 2h, i for all the 174 categories (terms) from DAVID
27 Bioinformatics Resources containing at least 2 confirmed hits and hypergeometric test *P*-values
28 < 0.05 . Details include source, number of confirmed hits, corresponding UniProtKB ID and gene
29 symbol, *P*-value, enrichment score ($-\log_{10}[P\text{-value}]$) and FDR adjusted *P*-value.

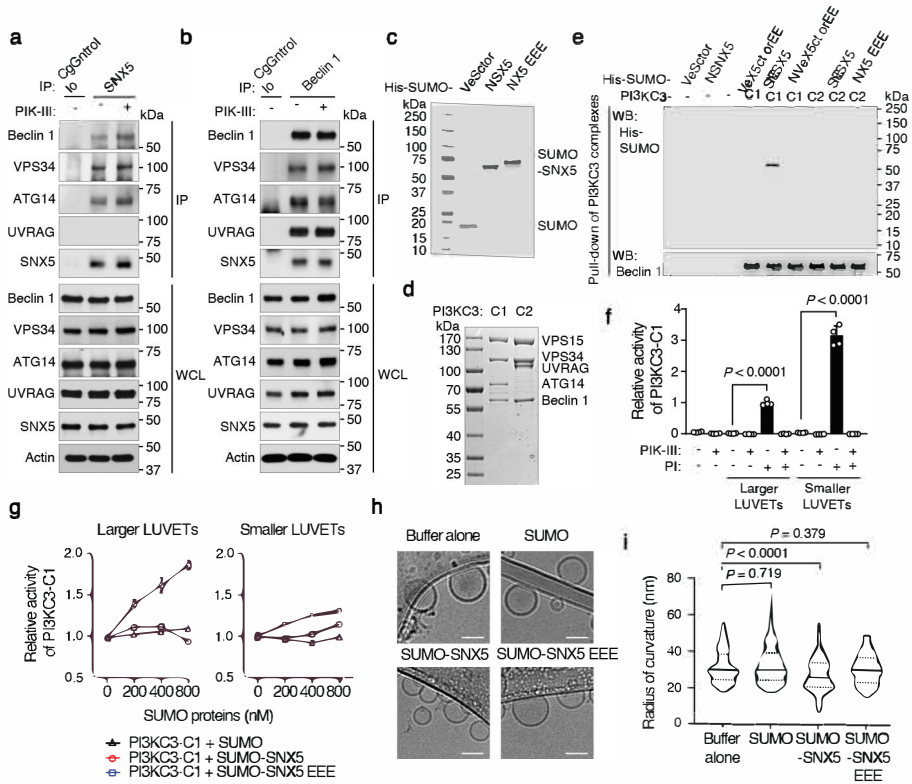
30

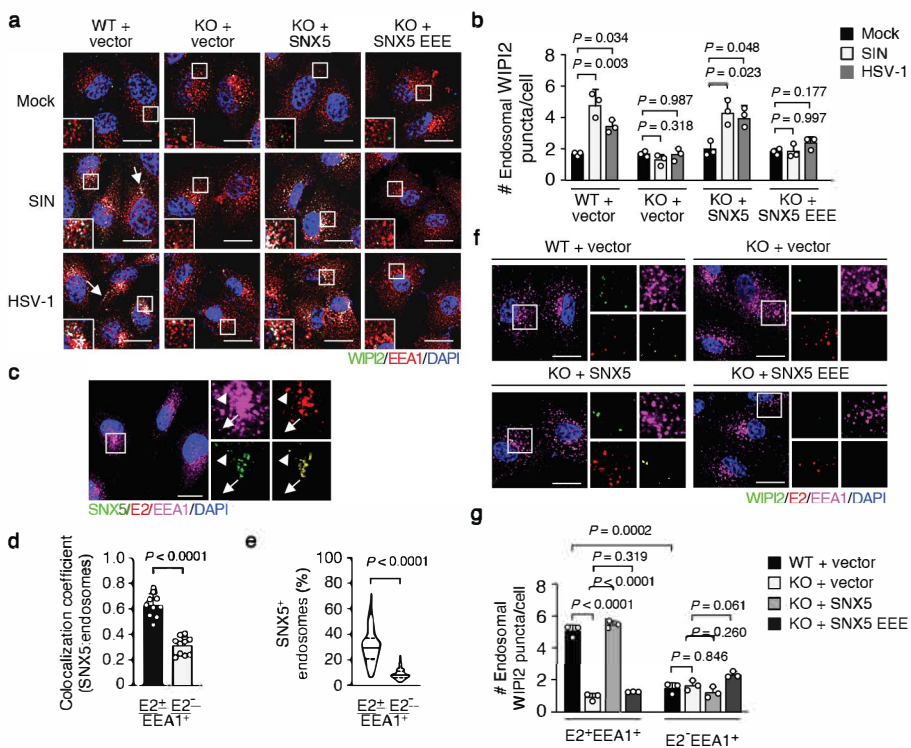
31 **Supplementary Figure 1.**

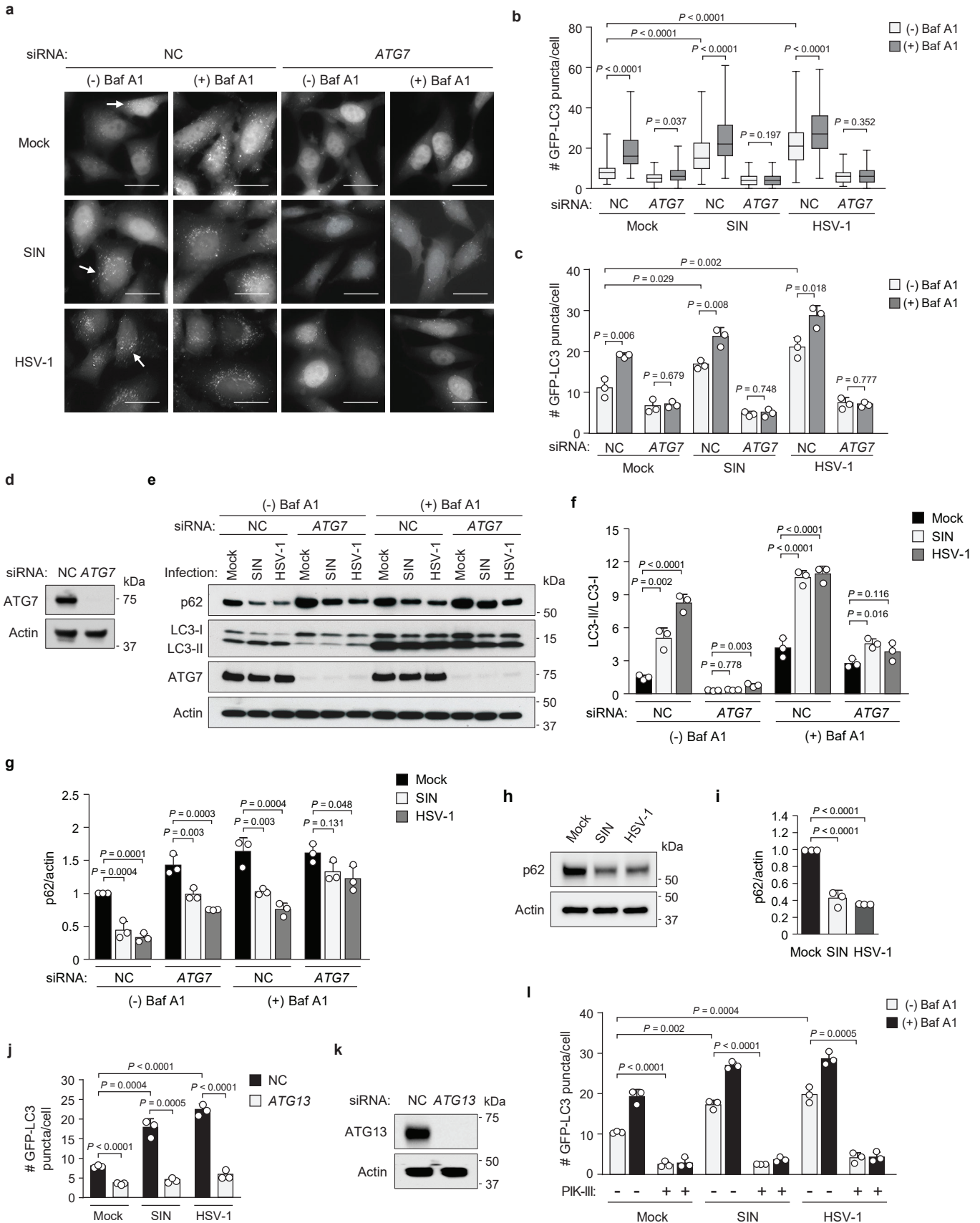
32 This file contains gel source data.

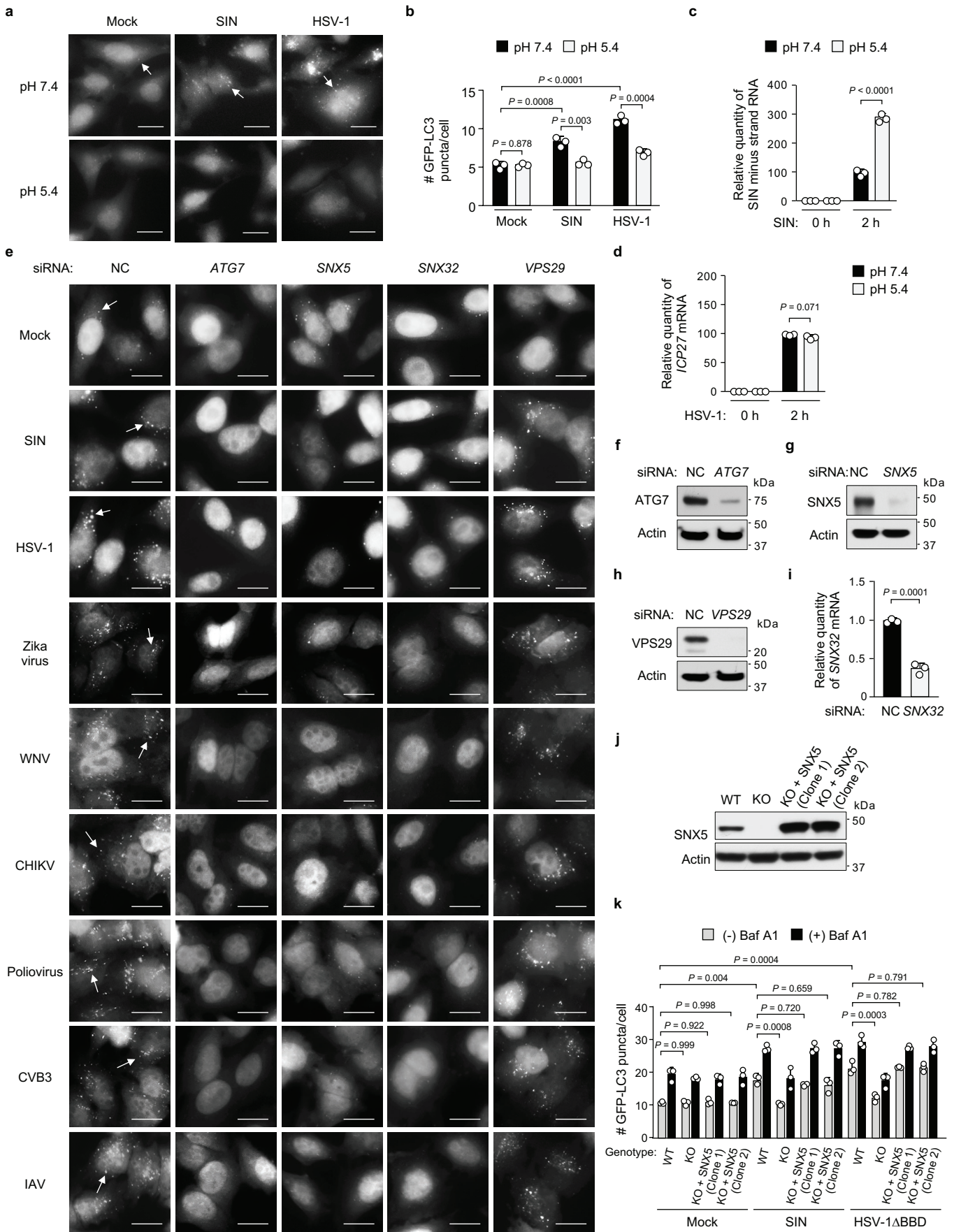
33

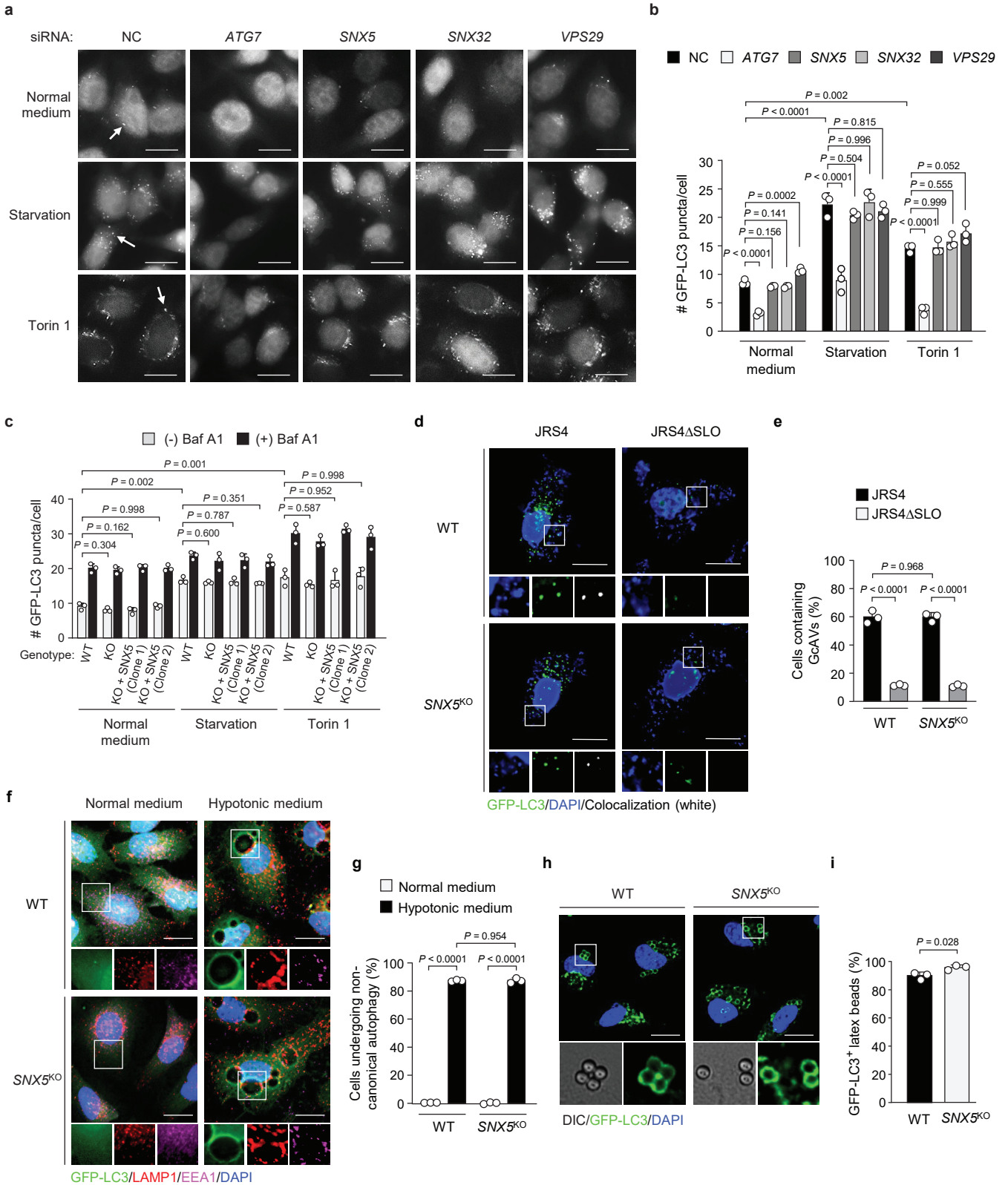


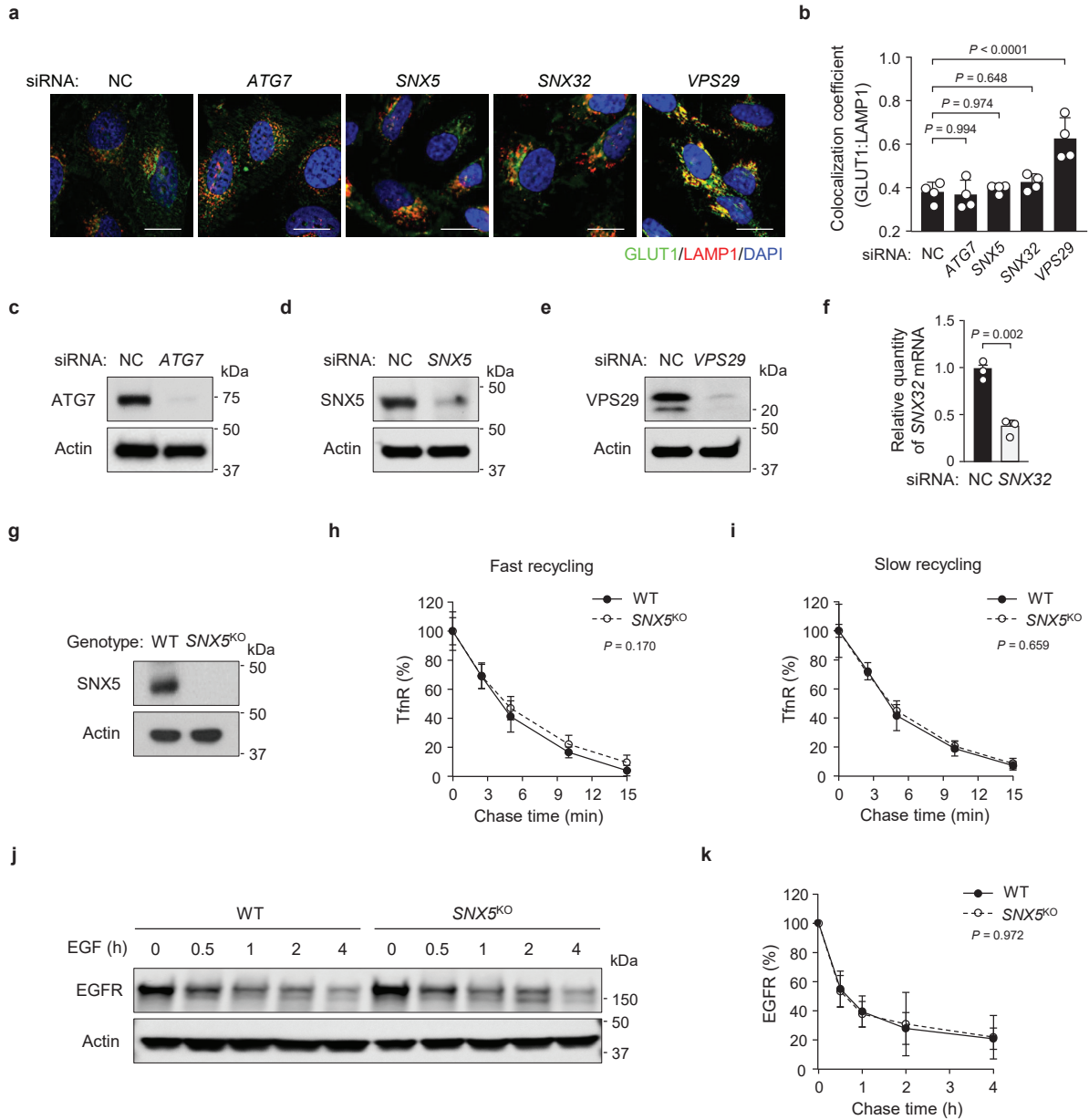


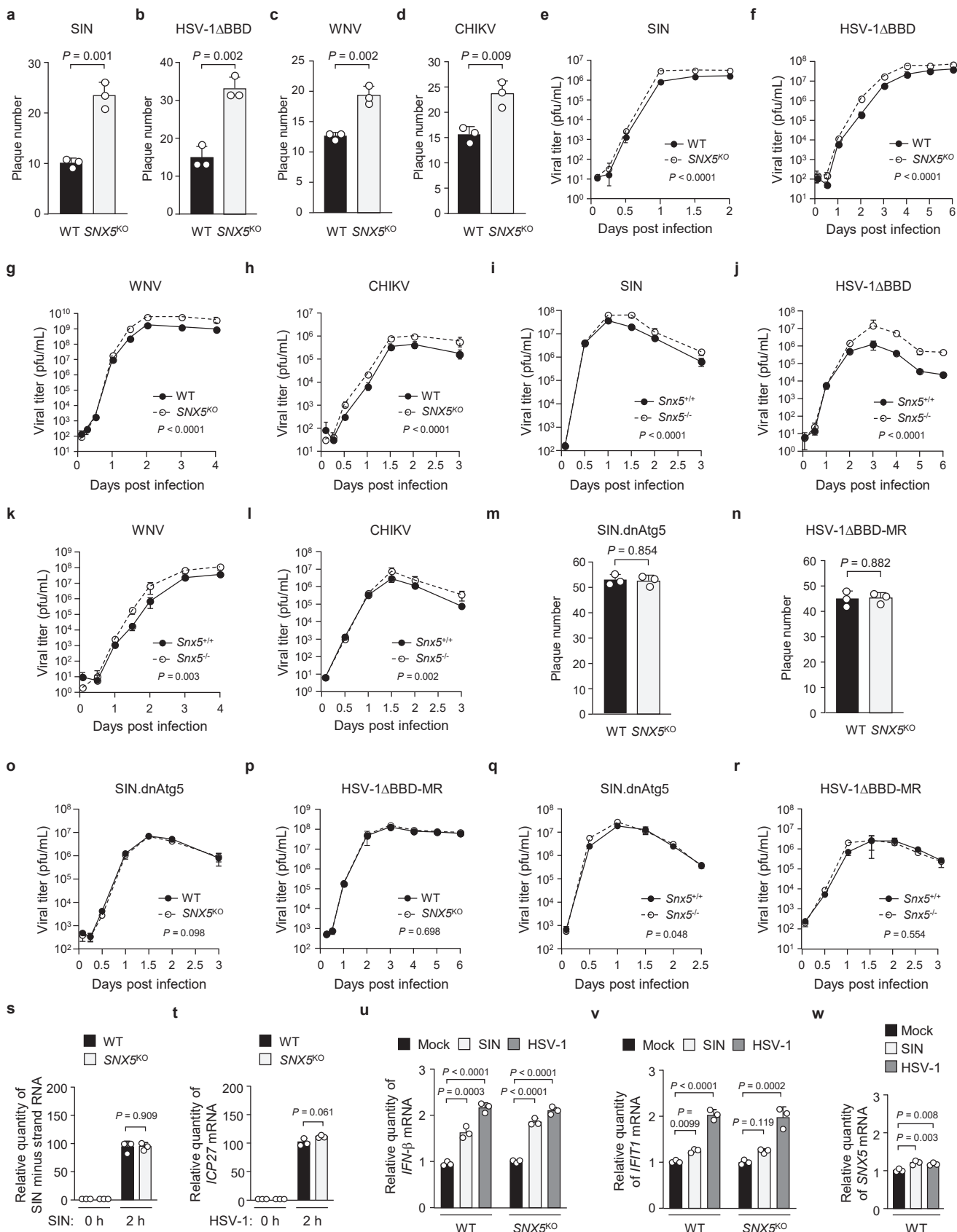


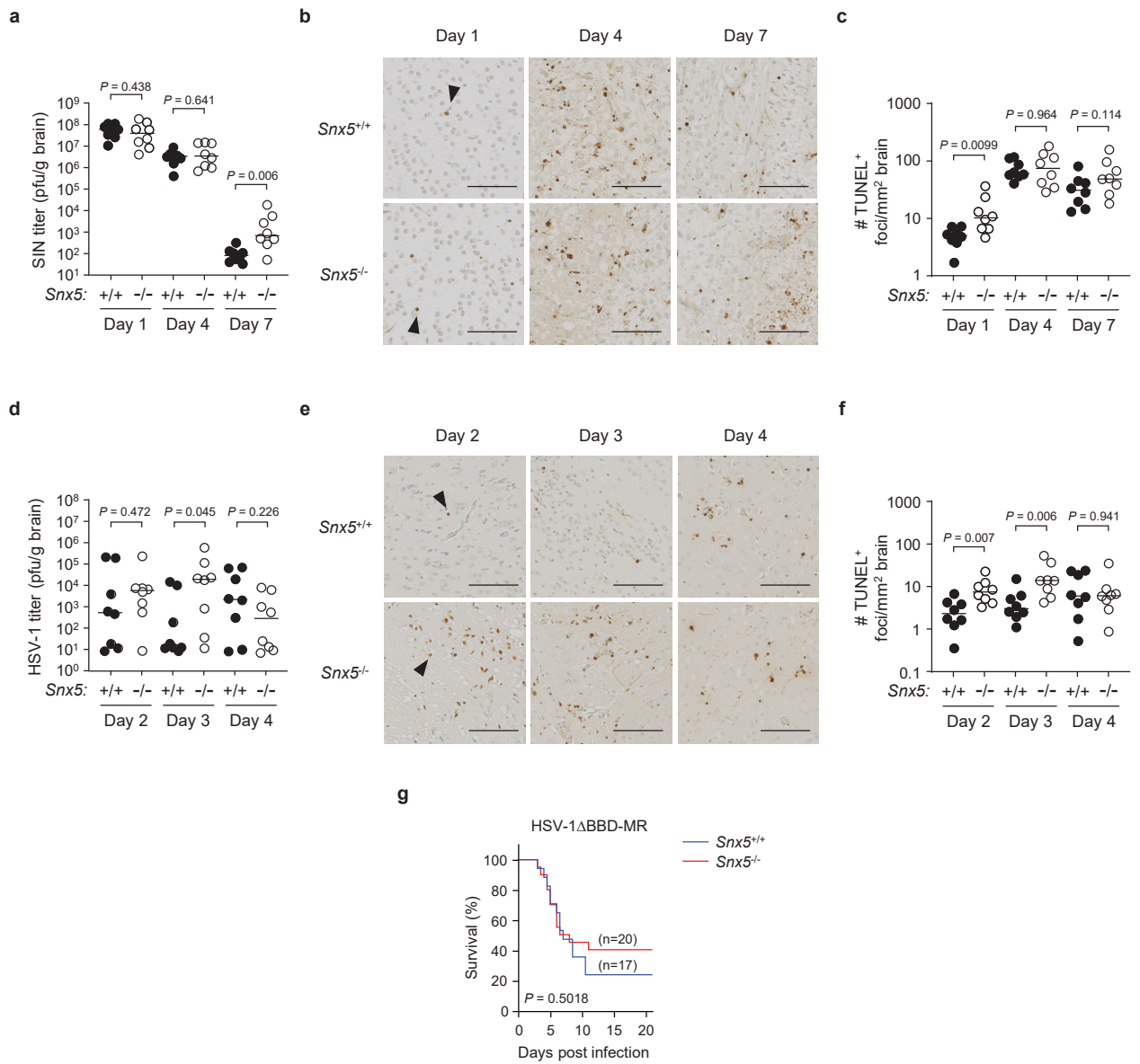


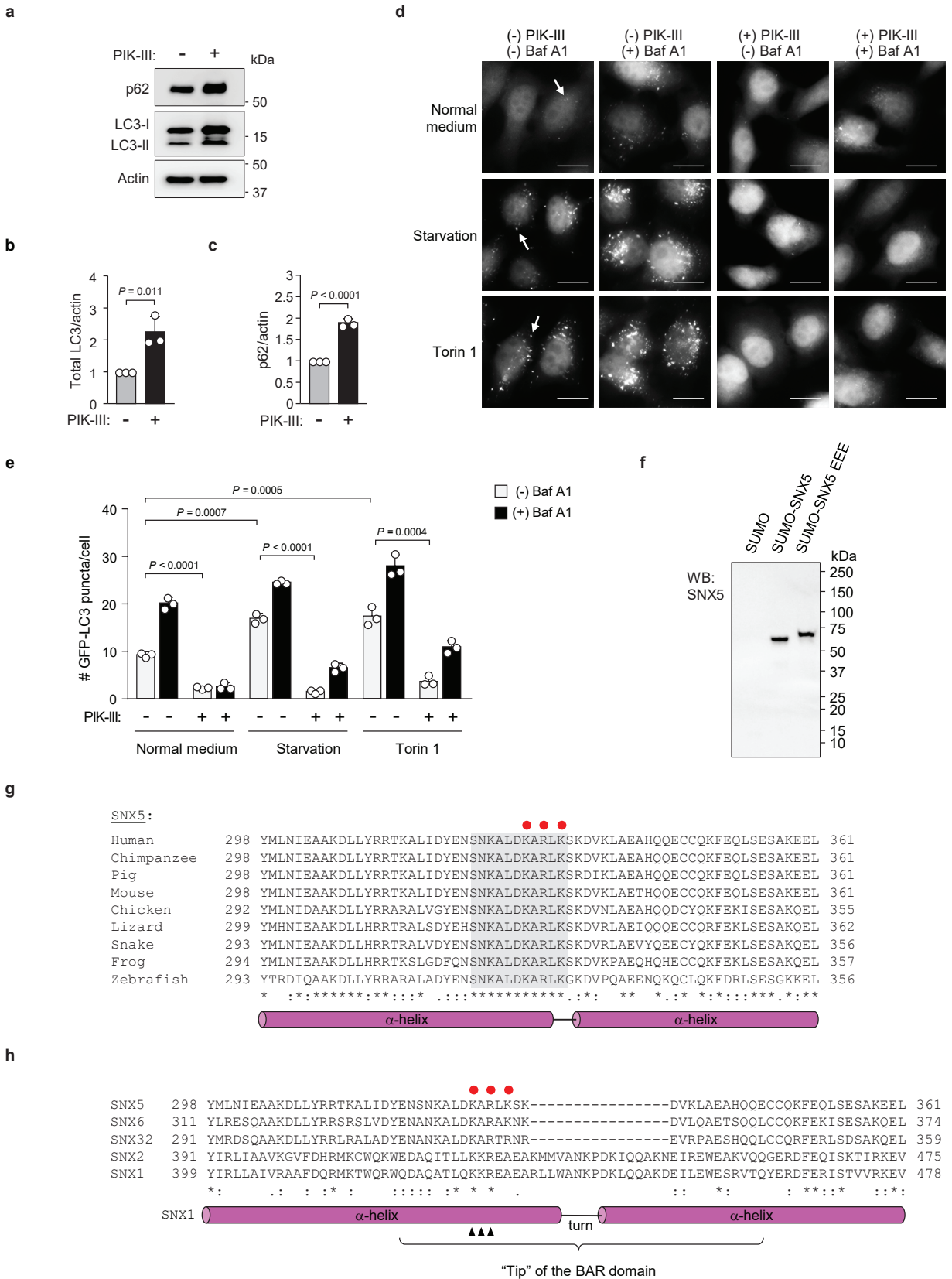


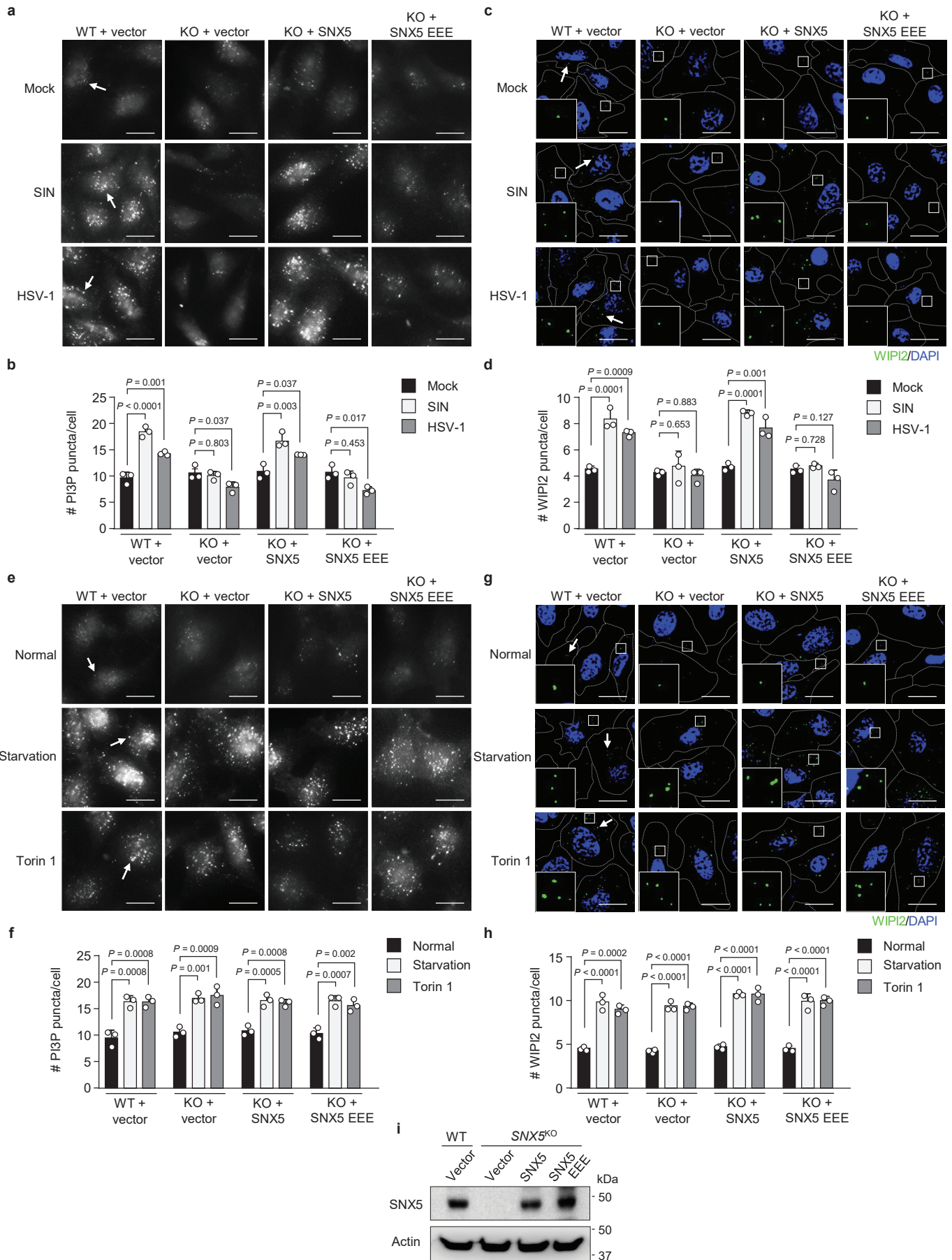




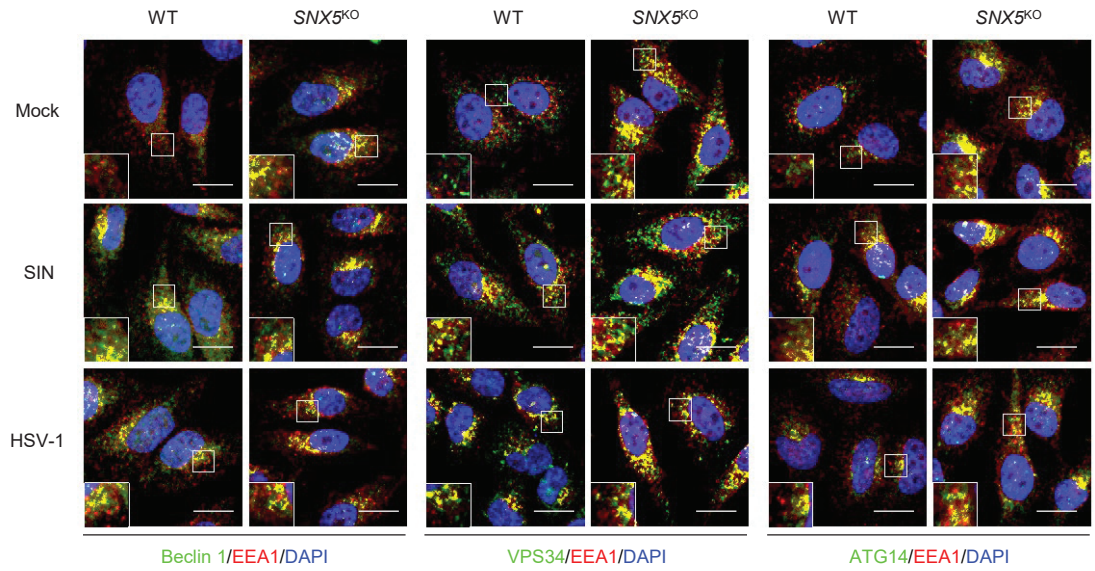




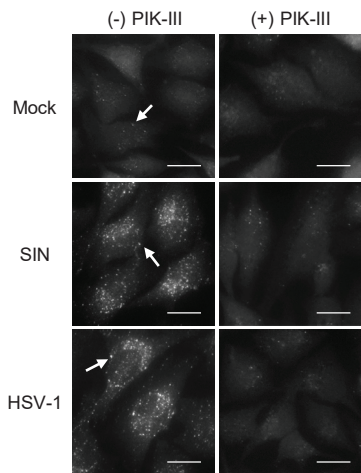




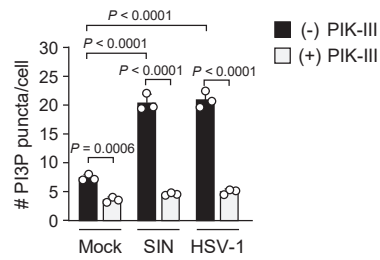
a



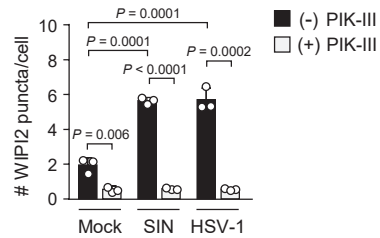
b



c



e



d

